

NEW ALGORITHMS FOR THE COMPILATION OF GLACIER INVENTORIES

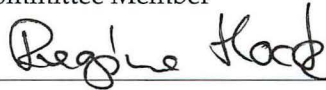
By

Christian Kienholz

RECOMMENDED:



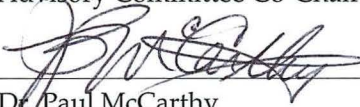
Dr. Franz Meyer
Advisory Committee Member



Dr. Regine Hock
Advisory Committee Co-Chair



Dr. Anthony Arendt
Advisory Committee Co-Chair

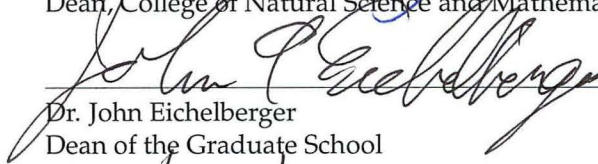


Dr. Paul McCarthy
Chair, Department of Geology and Geophysics

APPROVED:



Dr. Paul Layer
Dean, College of Natural Science and Mathematics



Dr. John Eichelberger
Dean of the Graduate School

11/28/13

Date

NEW ALGORITHMS FOR THE COMPILATION OF GLACIER INVENTORIES

A
THESIS

Presented to the Faculty
of the University of Alaska Fairbanks
in Partial Fulfillment of the Requirements
for the Degree of

MASTER OF SCIENCE

By
Christian Kienholz, M.S.

Fairbanks, Alaska

December 2013

Abstract

Glacier inventories are used for many applications in glaciology, however, their manual compilation is time-consuming. Here, we present two new algorithms for the automatic compilation of glacier inventories. The first approach is based on hydrological modeling tools and separates glacier complexes into individual glaciers, requiring a digital elevation model (DEM) and glacier complex outlines as input. Its application to $> 60,000$ km² of ice in Alaska (~98% success rate) and southern Arctic Canada (~97% success rate) indicates the method is robust if DEMs and glacier complex outlines of good quality are available. The second algorithm relies on glacier outlines and a DEM and derives centerlines in a three-step 'cost grid – least cost route' procedure. First, termini and heads are determined for every glacier. Second, centerlines are derived by determining the least cost route on a previously determined cost grid. Third, the centerlines are split into branches, followed by the attribution of a branch order. Application to $> 21,000$ Alaska glaciers shows that ~5.5% of the glacier heads and ~3.5% of the termini require manual correction. With corrected heads and termini, ~1.5% of the actual derived centerlines need edits. Comparison with alternative approaches reveals that the centerlines vary significantly depending on the algorithm used.

Table of Contents

	Page
Signature Page	i
Title Page	iii
Abstract	v
Table of Contents	vii
List of Figures	xi
List of Tables	xiii
Acknowledgements	xv
Chapter 1 General Introduction	1
Chapter 2 A new semi-automatic approach for dividing glacier complexes into individual glaciers	7
2.1 Abstract	7
2.2 Introduction	7
2.3 Methods	8
2.3.1 Overview	8
2.3.2 Glacier separation	9
2.3.2.1 Preprocessing	9
2.3.2.2 Identification of pour points	10
2.3.2.3 Flowshed calculation	10
2.3.2.4 Allocation of flowsheds to individual glaciers	10
2.3.2.5 Identification of sliver polygons	11
2.3.3 Error assessment	12
2.3.3.1 Preparation of reference outlines	12
2.3.3.2 Error allocation	13
2.3.4 Implementation	13
2.4 Application	13
2.4.1 Calibration	14
2.4.2 Validation	15
2.5 Discussion	17
2.5.1 Algorithm performance	17
2.5.2 Transferability of parameters	19
2.5.3 Error assessment	20

	Page
2.5.4 Previous algorithms	21
2.6 Conclusions	22
2.7 Acknowledgements	23
References	36
Chapter 3 A new method for deriving glacier centerlines applied to glaciers in Alaska and northwest Canada	39
3.1 Abstract	39
3.2 Introduction	39
3.3 Previous work	40
3.4 Test site and data	41
3.5 Method	42
3.5.1 Step 1 – Identification of glacier heads and termini	43
3.5.1.1 Glacier terminus	43
3.5.1.2 Glacier heads	43
3.5.2 Step 2 – Establishment of cost grid and determination of least cost route	44
3.5.2.1 Cost/penalty grid and route cost	44
3.5.2.2 Optimization	47
3.5.3 Step 3 – Derivation of branches and branch order	50
3.5.3.1 Branches	50
3.5.3.2 Branch order	51
3.5.4 Quality analysis and manual adjustments	52
3.5.5 Comparison to alternative methods	52
3.6 Results	53
3.7 Discussion	54
3.7.1 Algorithm	54
3.7.1.1 Termini	54
3.7.1.2 Heads	54
3.7.1.3 Cost grid – least cost route approach	55
3.7.1.4 Optimization	56
3.7.1.5 Branches and geometry order	56

	Page
3.7.2 Influence of DEM and outline quality	57
3.7.3 Quality assessment	58
3.7.4 Comparison to alternative methods	58
3.8 Conclusions	59
3.9 Acknowledgements	60
References	70
Chapter 4 General Conclusions	73

List of Figures

	Page
1.1 Main steps of a typical inventory workflow	3
2.1 Principle of basin separation using hydrological modeling tools	27
2.2 Diagram illustrating the conceptual workflow of the separation algorithm	28
2.3 Example showing the DEM gridcells of a glacier terminus including the surrounding buffer region	29
2.4 Location of pour points and corresponding flowsheds	30
2.5 Location of glacier complexes to which the new algorithm was applied	31
2.6 The number of misclassifications obtained in the Juneau Icefield test area as a function of the applied a and b values	32
2.7 Color-coded glacier outlines automatically derived for a subregion of the Western Alaska Range	33
2.8 Glacier basins for selected subregions of the Eastern Alaska Range (a–b), the Juneau Icefield (c), and the Western Chugach Mountains (d–e)	34
2.9 Failed automatic glacier separations in the Juneau Icefield area	35
2.10 Glacier separation of a mixed ice cap/valley glacier complex in Southern Arctic Canada	35
3.1 The study area comprising glaciers of Alaska and adjacent Canada	62
3.2 Automatically derived glacier heads (red crosses) and terminus (blue square) on Gilkey Glacier, Juneau Icefield, southeast Alaska	63
3.3 Three-step procedure to identify the heads of major glacier branches	64
3.4 Selected penalty grids of Gilkey Glacier and corresponding centerlines, using a constant a value of 4.25, but varying b	65
3.5 Elevation profile along a glacier centerline illustrating the definition of Δz_{up} and n_{up} for $I = 3$ sections	66
3.6 Illustration of the applied iteration threshold	66
3.7 The main processing steps illustrated using the example of Gilkey Glacier, Juneau Icefield	67
3.8 Derived centerlines for glaciers in the Stikine Icefield area	68

	Page
3.9 Histograms illustrating the length ratio distributions of differently derived glacier lengths	69

List of Tables

	Page
2.1 Test regions and their datasets	24
2.2 Calibrated parameters used in this study	25
2.3 Total number of glaciers in the test regions and number/fraction of misclassified glaciers	26
3.1 Used parameter values and units	61
3.2 Manual changes attributed to individual error categories	61

Acknowledgements

Thank you to NASA and NSF, the agencies that awarded funding for the work conducted in this master's project.

Thank you to my advisors Anthony Arendt, Regine Hock, and Franz Meyer, for having obtained funding to take me on as a graduate student. The collaboration during the last two years was both productive and very pleasant.

Thank you to Heinz Zumbühl, my former advisor and mentor at the University of Bern, for having enabled an exchange semester at UAF in 2009. This awakened my interest in Alaska, which was an important reason to come back as a graduate student.

Thank you to Peter Mani, director at *geo7*, who understood my desire to gain more experience beyond Switzerland's borders and outside of the geohazard field. It has been worth it so far.

Thank you to my family, especially my parents and my brothers Peter and Mathias, for all the support and fun so far. A great thanks to where you are these days – Bern, Perth, and Sydney!

Chapter 1

General Introduction

Information derived from glacier inventories is used for virtually all glaciological applications. Most fundamentally, the comparison of glacier inventories of different dates allows quantification of glacier changes, which is important to better understand the complex behavior of glaciers in space and time. Specifically, glacier outlines from inventories are required for extrapolation of *in situ* mass balance data to entire glaciers (Paterson, 1994) and estimation of glacier volumes using empirical volume-scaling techniques (Bahr et al., 1997; Radić and Hock, 2010) or physically based approaches (Huss and Farinotti, 2012; Linsbauer et al., 2012); in addition, they are required for modelling the future evolution of glaciers (Radić and Hock, 2011).

Because the non-automated derivation of glacier inventories is very time-consuming, accurate large-scale inventories have remained incomplete (e.g., Ohmura, 2009). Within the last decade, considerable efforts have been undertaken to automatically outline glacier complexes from satellite imagery, which is the first main step in a typical workflow to compile inventory data (Fig. 1.1; Paul et al., 2002; Kargel et al., 2005; Paul et al., 2004; Raup et al., 2007; Racoviteanu et al., 2009). Glacier complexes indicate the presence or absence of glacier ice, that is, they do not distinguish individual glacier entities. However, as many studies require the outlines of individual glaciers, it is paramount to split glacier complexes into individual glaciers, which is the second main step of a typical inventory workflow. While this can be done manually by analyzing flow fields or Digital Elevation Models (DEMs), an automated workflow would be desirable to reduce the amount of manual work. Little work has been published with regard to this second step (Manley, 2008; Schiefer et al., 2008; Bolch et al., 2010).

The third step of the inventory workflow is to use glacier outlines to derive dimensional characteristics such as area, average slope, and aspect for each glacier individually. While most of these parameters can be derived in a straightforward way by combining the glacier outlines with a DEM, the derivation of the parameter glacier length (usually defined as the length of the longest glacier centerline) is considered challenging (Paul et al., 2009). To obtain accurate glacier lengths, centerlines are often digitized manually (e.g., Nuth et al., 2013), which is very time-consuming. Simple fully automated approaches tend to be prone to large uncertainties (Schiefer et al., 2008), and more sophisticated approaches are currently rare (Le Bris and Paul, 2013). Therefore, it would be desirable to have an au-

tomated approach for deriving accurate centerlines. These centerlines could be used not only to derive glacier length, but also for length change analyses, flowline modelling and the extrapolation of laser altimetry profiles to entire glaciers.

The overarching goal of this project is to further automate the compilation of glacier inventories. Given the foci of previous research, we here focus on steps two and three of the inventory workflow (Fig. 1.1) and aim to create automated workflows to:

1. split glacier complexes into single glaciers, and
2. generate glacier centerlines.

The two distinct goals have resulted in two papers. The paper 'A new semi-automatic approach for dividing glacier complexes into individual glaciers' was published in the *Journal of Glaciology*, and the second paper 'A new method for deriving glacier centerlines applied to glaciers in Alaska and northwest Canada' has been submitted to *The Cryosphere*.

Methods and concepts for both papers have been developed by the main author Christian Kienholz, who also wrote the original manuscripts. Justin Rich came up with the initial concept for the second paper. All co-authors (Justin Rich, Anthony Arendt, Regine Hock) discussed the methods throughout the development stages and edited the paper drafts.

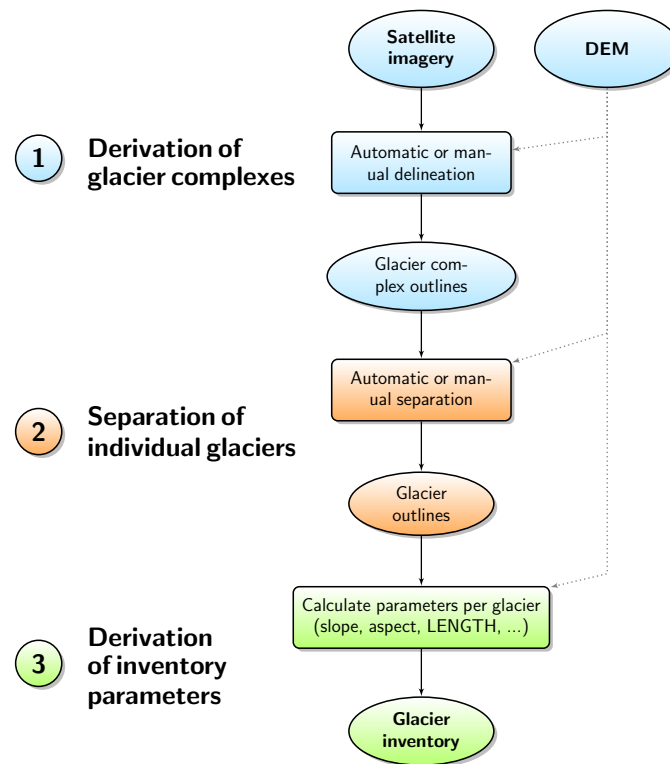


Figure 1.1. Main steps of a typical inventory workflow. The conducted work focuses on steps 2 and 3.

References

- Bahr, D., M. Meier, and S. Peckham (1997). The physical basis of glacier volume-area scaling. *Journal of Geophysical Research* 102(B9), 20355–20362.
- Bolch, T., B. Menounos, and R. Wheate (2010). Landsat-based inventory of glaciers in western Canada, 1985–2005. *Remote Sensing of Environment* 114(1), 127–137.
- Huss, M. and D. Farinotti (2012). Distributed ice thickness and volume of all glaciers around the globe. *Journal of Geophysical Research* 117(F4), F04010.
- Kargel, J., M. Abrams, M. Bishop, A. Bush, G. Hamilton, H. Jiskoot, A. Kääb, H. Kieffer, E. Lee, F. Paul, et al. (2005). Multispectral imaging contributions to global land ice measurements from space. *Remote Sensing of Environment* 99(1), 187–219.
- Le Bris, R. and F. Paul (2013). An automatic method to create flow lines for determination of glacier length: A pilot study with Alaskan glaciers. *Computers & Geosciences* 52, 234–245.
- Linsbauer, A., F. Paul, and W. Haeberli (2012). Modeling glacier thickness distribution and bed topography over entire mountain ranges with glabtop: Application of a fast and robust approach. *Journal of Geophysical Research* 117(F3), F03007.
- Manley, W. (2008). Geospatial inventory and analysis of glaciers: A case study for the eastern Alaska Range. In R. S. Williams and J. G. Ferrigno (Eds.), *Satellite image atlas of glaciers of the world*. U.S. Geological Survey Professional Paper 1386-E, 525 pp.
- Nuth, C., J. Kohler, M. König, A. von Deschanden, J. O. Hagen, A. Kääb, G. Moholdt, and R. Pettersson (2013). Decadal changes from a multi-temporal glacier inventory of Svalbard. *The Cryosphere Discussions* 7(3), 2489–2532.
- Ohmura, A. (2009). Completing the World Glacier Inventory. *Annals of Glaciology* 50(53), 144–148.
- Paterson, W. S. B. (1994). *The Physics of Glaciers*. 3rd edition. Elsevier Science, Oxford, 481 pp.
- Paul, F., R. G. Barry, J. G. Cogley, H. Frey, W. Haeberli, A. Ohmura, C. S. L. Ommanney, B. Raup, A. Rivera, and M. Zemp (2009). Recommendations for the compilation of glacier inventory data from digital sources. *Annals of Glaciology* 50(53), 119–126.

Paul, F., C. Huggel, and A. Kääb (2004). Combining satellite multispectral image data and a digital elevation model for mapping debris-covered glaciers. *Remote Sensing of Environment* 89(4), 510–518.

Paul, F., A. Kääb, M. Maisch, T. Kellenberger, and W. Haeberli (2002). The new remote sensing derived Swiss glacier inventory: I. Methods. *Annals of Glaciology* 34, 355–361.

Racoviteanu, A., F. Paul, B. Raup, S. Khalsa, and R. Armstrong (2009). Challenges and recommendations in mapping of glacier parameters from space: results of the 2008 global land ice measurements from space (glims) workshop, boulder, colorado, usa. *Annals of Glaciology* 50(53), 53–69.

Radić, V. and R. Hock (2010). Regional and global volumes of glaciers derived from statistical upscaling of glacier inventory data. *Journal of Geophysical Research* 115, F01010.

Radić, V. and R. Hock (2011). Regionally differentiated contribution of mountain glaciers and ice caps to future sea-level rise. *Nature Geoscience* 4(2), 91–94.

Raup, B., A. Kääb, J. S. Kargel, M. P. Bishop, G. Hamilton, E. Lee, F. Paul, F. Rau, D. Soltesz, S. J. S. Khalsa, M. Beedle, and C. Helm (2007). Remote sensing and GIS technology in the Global Land Ice Measurements from Space (GLIMS) Project. *Computers & Geosciences* 33(1), 104–125.

Schiefer, E., B. Menounos, and R. Wheate (2008). An inventory and morphometric analysis of British Columbia glaciers, Canada. *Journal of Glaciology* 54(186), 551–560.

Chapter 2

A new semi-automatic approach for dividing glacier complexes into individual glaciers¹

2.1 Abstract

Many glaciological and hydrological studies require outlines of individual glaciers rather than total ice cover. Here we develop a new semi-automatic algorithm that uses a digital elevation model (DEM) and outlines of glacier complexes to calculate the extents of individual glaciers. The algorithm first applies hydrological modeling tools to a modified DEM to calculate flowsheds. It then merges flowsheds that belong to individual glaciers using a distance-based approach, whose required empirical parameters are derived from the Juneau Icefield area in Alaska. In this region, 2% of ~1300 glaciers were misclassified. The algorithm was validated on >25,000 km² of ice in other regions in Alaska and on >40,000 km² of ice in Arctic Canada, resulting in ~2% and ~3% misclassified glaciers, respectively. Results indicate that the algorithm is robust provided the DEM and the outlines are of good quality.

2.2 Introduction

Considerable progress has been made towards delineating the extent of the Earth's glaciers, mainly within the scope of the Global Land Ice Measurements from Space (GLIMS) program (Kargel et al., 2005; Raup and Khalsa, 2007). Glacier outlines are typically derived from optical space- or airborne data by (semi-)automated techniques or by manual digitization (Paul et al., 2002; Paul et al., 2004; Raup and Khalsa, 2007; Racoviteanu et al., 2009). The first step in assembling glacier outlines is to identify the presence or absence of glacier ice, which in turn allows the computation of total ice cover. The resulting outlines often include glacier complexes, i.e., collections of glaciers that meet at ice divides.

Many studies require not only knowledge of total regional ice extent, but also the outlines and areas of individual glaciers. For example, individual glacier outlines are required for accurate extrapolation of point geodetic or *in situ* data to arrive at glacier-wide mass balances. Volume-area scaling techniques (Bahr et al., 1997) used to assess regional or global ice volumes (Radić and Hock, 2010) or to project future glacier evolutions (Radić and Hock, 2011) also require accurate glacier areas. Individual glacier outlines are also necessary for physically based approaches used to calculate regional (Linsbauer et al., 2012)

¹Kienholz, C., R. Hock, and A. A. Arendt (2013). *Journal of Glaciology* 59 (217), 913–925.

or global ice volumes (Huss and Farinotti, 2012). Beedle et al. (2008) quantify the effects on glaciological applications that arise from using different glacier outlines.

Manual glacier separation by visual inspection of ice flow patterns is time-consuming and difficult, especially in terrain with low slope. To date, three semi-automatic algorithms have been developed to separate glacier complexes, all of which rely on a DEM and hydrological modeling tools (Manley, 2008; Schiefer et al., 2008; Bolch et al., 2010; see Racoviteanu et al. (2009) for a review). Because these algorithms are part of broader inventory studies, explanations of the algorithms and corresponding error assessments are brief. However, these approaches require manual intervention to some extent, in most cases to correct misclassified glaciers. Here we present a new algorithm that aims at minimizing the amount of manual intervention, with the ultimate goal of having a standardized, automated approach capable of coping with a wide range of glacier types. Similar to previous approaches, our algorithm requires a DEM and outlines of glacier complexes as input. Our method is novel in that it takes additional steps to automate the identification of individual glaciers. We test the method on glacier complexes in Alaska, USA and southern Arctic Canada, and show that for these areas the algorithm performs well and requires little manual correction. To quantify the performance of our algorithm, we use a semi-automatic approach with reproducible results. The presented algorithm is available for use or as a basis for further development.

2.3 Methods

2.3.1 Overview

Like previous automated tools (Racoviteanu et al., 2009), the core of our algorithm is based on hydrological modeling tools readily implemented in many established Geographic Information Systems (GIS). These tools map the watershed area that contributes surface flow to a common drainage outlet point ('pour point'; e.g., the site of a river gauging station). By relying on watershed algorithms we implicitly assume that ice divides, topographic divides, and hydrological divides are identical, which holds true for most glaciers in confined valleys (Manley, 2008; Schiefer et al., 2008; Bolch et al., 2010).

For the identification of pour points, there are differences between glacierized and unglacierized basins that must be considered. In unglacierized river basins, pour points generally coincide with the lowest point of the valley cross-section, which makes the calculation of watersheds straightforward (Fig. 2.1a). However, due to the convex surface of

glacier ablation areas, not all ice of the same glacier converges to a single point. Thus, taking the lowest glacier point as the pour point does not necessarily capture the entire surface area of a glacier (Fig. 2.1b). Hence, multiple pour points may be required to capture the entire glacier surface (Fig. 2.1c). The identified ‘flowsheds’, one flowshed per pour point, also need to be allocated to individual glaciers in order to obtain the correct outline of each individual glacier within a glacier complex (Fig. 2.1d). Our algorithm automatically identifies pour points and merges flowsheds associated with individual glaciers.

2.3.2 Glacier separation

The glacier separation workflow consists of five main steps: (1) preprocessing, (2) identification of pour points, (3) flowshed calculation, (4) allocation of flowsheds to individual glaciers and (5) identification of sliver polygons. Fig. 2.2 illustrates the conceptual workflow. Some of the required empirical parameters have fixed values, others are obtained through calibration.

2.3.2.1 Preprocessing

We begin with a DEM of a region encompassing all terrain surrounding the glacier complex of interest. As the native resolution and quality of provided DEMs varies, we resample the DEM to a fixed resolution and apply a smoothing filter. In order to constrain our subsequent watershed calculations to the glacierized terrain, it is necessary to extract only those DEM gridcells contained within the outline of the glacier complex. Before performing this extraction, we create a new outline to extend the glacier boundary several DEM gridcells beyond the outer edge of the glacier complex polygon, a procedure known as ‘buffering’ in GIS terminology (buffer1, Fig. 2.3). The buffering of our glacier complex enables us to build an artificial ‘gutter’ of depth L_{gutter} that extends beyond the outer edge of the glaciers, located at a fixed distance from the glacier complex (buffer2), and that has a magnitude less than buffer1. This process forces flow from upstream regions in the watershed to terminate in the gutter, which in turn reduces the number of pour points, and constrains the pour points to lower glacier elevations. We set the gutter some distance outside the actual glacier complex in order to make sure none of the gridcells of the gutter contain any ice. Thereby, we avoid changing the topography of the glacierized terrain.

2.3.2.2 Identification of pour points

Next we use GIS tools to calculate the accumulated flow to each gridcell of the gutter (Fig. 2.3). The accumulated flow measures the number of upstream gridcells contributing flow to a certain cell, where high values indicate a large contributing area. The accumulated flow along the gutter is then used to locate pour points that are needed to identify individual glaciers. We exploit the fact that pour points correspond to local flow accumulation maxima. For each cell along the gutter we compare flow accumulation values to the neighboring flow accumulation values. If the local flow accumulation value is higher than the flow accumulation of its neighbors, the cell is considered a pour point.

2.3.2.3 Flowshed calculation

In the next step, contributing areas (watersheds) are calculated using standard GIS functions. These functions use calculations of flow direction, derived from the DEM, to identify as a single watershed all gridcells that contribute flow to a pour point. We iterate through the pour points in order of decreasing flow accumulation and calculate the watersheds for each pour point individually. During each iteration, we also check for potential pour points located within the calculated watershed. Such points are removed (not used to calculate watersheds) because they lie above the pour point that was used to calculate the watershed. This step prevents the final watersheds from being split unnecessarily. We then convert the final watersheds, represented as gridded maps, to vector polygons, and smooth the polygons to remove jagged edges that occur in the grid-to-vector conversion. As a final step, we overlay the watersheds which extend a short distance beyond the glacier edge with the original glacier complex polygon, yielding the glacierized portion of the watershed (i.e., the flowshed).

2.3.2.4 Allocation of flowsheds to individual glaciers

The fact that glaciers do not flow in the same manner as liquid water means that standard GIS watershed functions will often produce more than one flowshed per glacier (Fig. 2.1). Therefore, our next step is to develop a simple method for grouping flowsheds based on pour point topology. Experimenting with numerous distance-based approaches resulted in a workflow that begins with building circles around each pour point (Fig. 2.4). These circles are eventually used to decide whether adjacent flowsheds need to be merged to-

gether. The radius of each circle, R (m), is defined as an increasing function of the flow accumulation, F , at that point,

$$R = a \cdot F^b. \quad (2.1)$$

This equation is based on the idea that we need larger radii to identify the flowsheds of larger glaciers. We exploit the fact that the flow accumulation increases with the size of the glacier. An exponential relationship with two scaling parameters a and b is used based on testing carried out during algorithm calibration. A threshold c constrains the radius R to an explicitly defined maximum size.

Next we determine the section of the circle that is covered by glacier ice, P_{glac} (Fig. 2.4), and check whether one or more adjacent flowsheds are overlain by P_{glac} . The overlain flowsheds are merged as we assume they belong to the same glacier. This procedure is carried out for every pour point separately by incrementally looping through the pour points. In some cases, P_{glac} consists of multiple disconnected sections completely separated by unglacierized terrain (e.g., if R is sufficiently large to reach into disconnected flowsheds). In this case, we proceed only with the section of P_{glac} whose perimeter is closest to the pour point and ignore any other disconnected sections of P_{glac} .

2.3.2.5 Identification of sliver polygons

The previous step produces a dataset with flowsheds allocated to individual glaciers. This dataset typically contains ‘sliver polygons’, i.e., small, elongate features located mostly along mountain ridges. With their small area and characteristic shape, slivers are typically not considered distinct glaciers (e.g., Frey et al., 2012). In fact, sliver polygons are often artifacts due to DEM or outline inaccuracies, or due to relative shifts between the two datasets. To remove sliver polygons, we merge polygons identified as slivers with the neighboring polygon with the longest shared boundary. Previous approaches deal with sliver polygons by setting minimum area thresholds (e.g., Schiefer et al., 2008). We follow this approach and use a value of A_{sliver1} below which all polygons are identified as slivers. Our analysis of algorithm performance showed that not all slivers were identified this way. Therefore, we use an additional criterion, glacier compactness, which is defined as the perimeter of a circle with the area of the glacier divided by the actual measured glacier perimeter (Allen, 1998). In addition to the above criterion A_{sliver1} , we identify polygons as

slivers if they have an area less than the threshold $A_{\text{sliver}2}$ and, concurrently, a compactness parameter less than the threshold C_{sliver} . Using the thresholds $A_{\text{sliver}2}$ and C_{sliver} , we exploit the fact that sliver polygons typically have small areas along with low compactness values due to their elongate shape.

Polygons lacking a shared boundary with a neighboring glacier or not fulfilling the above criteria are considered individual glaciers, which maintains the initial area of the glacier complex.

2.3.3 Error assessment

The error assessment consists of two main steps: (1) preparation of reference outlines and (2) error allocation. We quantify errors if glaciers are split or merged incorrectly. We do not assess errors that are only due to DEM inaccuracies. Inaccurate DEMs lead to topographic divides that are different from the true topographic divides, which ultimately results in shifted glacier divides. Because such errors do not directly reflect algorithm failure, they are not assessed here.

2.3.3.1 Preparation of reference outlines

Quantifying errors in our separation algorithm requires a set of reference outlines against which we compare our output. While it would be best to use a fully independent dataset, none exist that would not introduce additional uncertainties due to, for example, differences in technician interpretation. Although they are not fully independent, we use reference data obtained by careful manual checking of our own 'raw' algorithm output, using contours, shaded relief DEMs, and airborne/spaceborne imagery. We visually check and adjust outlines if a glacier tongue remains split, or if glaciers are merged erroneously. Sliver polygons, undetected by the algorithm, are also merged. However, we do not move glacier boundaries in the accumulation areas that are due to DEM errors rather than algorithm failure. The adjusted reference glacier outlines are used to derive a point dataset that contains one centroid point for every glacier, i.e., one point centrally located within the perimeter of each individual glacier. We then use these centroid points as a basis for counting numbers of errors in our dataset.

2.3.3.2 Error allocation

We combine the above point dataset with the raw glacier outlines and determine the number of points located within the perimeter of each glacier of the raw glacier outlines. This number of points allows us to derive the number of errors,

$$N_{\text{error}} = \sum_{i=1}^z |n_i - 1| \quad (2.2)$$

where N_{error} is the total number of errors, n_i is the number of points within the i th glacier of the raw glacier outlines, and z is the total number of glaciers in the dataset. A glacier that contains one point ($n = 1$) exists in both the raw and the reference glacier outlines, and no error is added to N_{error} . A glacier that contains no points ($n = 0$) was merged with another glacier during the visual check and one error is added. A glacier that contains more than one point ($n > 1$) was split into multiple glaciers during the visual check and $n - 1$ errors are added to N_{error} . For example, if the algorithm merged three glaciers that should be separate according to the reference outlines, three points ($n = 3$) are found within the perimeter of this specific glacier, and two errors are added to N_{error} . All glacier outlines contributing errors are stored separately by assigning them to two datasets, ‘split incorrectly’ (if $n = 0$) or ‘merged incorrectly’ (if $n > 1$), which allows a statistical analysis of these outlines. To obtain relative errors, N_{error} is divided by the total number of glaciers determined by the algorithm.

2.3.4 Implementation

The glacier separation algorithm is written in the *Python*TM programming language and uses functions of the Environmental Systems Research Institute *ESRI*[®] *ArcGIS 10.1* software package. This algorithm can be run from an integrated development environment or from inside *ArcGIS*. For larger regions we use a parent script that splits the domain into several subregions and launches the actual script for each of these subregions. The error assessment workflow is also implemented in a *Python*TM script.

2.4 Application

The algorithm was applied to several glacier complexes in Alaska ($\sim 30,000 \text{ km}^2$, Fig. 2.5a) and southern Arctic Canada ($\sim 40,000 \text{ km}^2$, Fig. 2.5b). The regions include a variety of

glacier types ranging from small valley glaciers to large ice fields and ice caps. Details about the areas and datasets used are given in Table 2.1. Quality and native resolution of the used outlines and DEMs vary substantially among the regions. For example, Alaska’s National Elevation Dataset (NED) DEM has non-systematic horizontal and vertical offsets and is out of date due to substantial changes in glacier extent and topography that have occurred since its compilation in the 1950s.

2.4.1 Calibration

In total, ten parameters (Table 2.2) were derived for the Juneau Icefield area (Fig. 2.5a), applying trial-and-error experiments as well as automatized calibration. We used a DEM resampled to a spatial resolution of 40 m. Our experiments showed that this cell spacing retains large-scale relief features and allows for deriving reasonably accurate and smooth flowsheds. For buffer1, we used 160 m (4 cells) and for buffer2, we chose 80 m (2 cells) in order to make sure that none of the glacierized terrain is affected by the creation of the gutter. Trial-and-error procedures showed that an L_{gutter} of 100 m was sufficient to significantly reduce the number of pour points and to constrain them to lower glacier portions. The parameters A_{sliver1} , A_{sliver2} , and C_{sliver} were determined through visual inspection of raw tool output. In the case of A_{sliver1} , we consulted reference values from previous studies. Our A_{sliver1} of 100,000 m² follows Schiefer et al. (2008) and is higher than corresponding values used in other studies. For example, Bolch et al. (2010) and Frey et al. (2012) used thresholds of 50,000 m² and 20,000 m², respectively.

The above parameters were kept fixed during the next sequence of steps initiated by defining the radius R in terms of the flow accumulation, F . A linear relationship between R and F proved unfeasible due to the large spread of the flow accumulation values. In the case of the Juneau Icefield area, the flow accumulation of the obtained pour points ranged between < 100 and $> 428,000$ cells, which suggested an exponential or logarithmic relationship between R and F . We ultimately used the exponential Equation (2.1) with parameters a and b . Threshold c was introduced concurrently to constrain the maximum value of R . We set the c threshold to 3500 m and proceeded with determining the parameters a and b . By visual inspection, we derived two preliminary a and b values. In practice, we ran the glacier separation algorithm until step 3, ‘flowshed calculation’ (Fig. 2.2). Next we measured minimal radii required to merge flowsheds that belong together, and maximal radii allowed to keep separate flowsheds apart. This resulted in pour points that had flow accu-

mulation, radius and category ('maximum', 'minimum') values allocated. Visually fitting a curve to the resulting point cloud led to the preliminary values for a and b . For the actual calibration of a and b , we used a workflow similar to the error assessment. We first created a set of reference glacier outlines by running the glacier separation algorithm using the preliminary a and b values. We then visually checked and manually adjusted these outlines. Next, we ran the code multiple times, varying the parameters a and b . Each time, we determined the number of errors using Equation (2.2). Fig. 2.6 shows the resulting error surfaces with the a and b parameters on the x - and y -axes. The panels distinguish the error categories. A smaller P_{glac} , i.e., smaller a and b values, leads to a decreasing number of errors in the category 'merged incorrectly' (Fig. 2.6a). In fact, as P_{glac} decreases, the number of mergers decreases overall, including wrong mergers. Concurrently, the number of errors in the category 'split incorrectly' increases (Fig. 2.6b), because a smaller P_{glac} leaves flowsheds split that should be merged. Fig. 2.6c (total misclassifications) illustrates this compromise involved in choosing optimal a and b pairs. We selected 14.3 m for parameter a , and 0.5 for b , which corresponds to a local minimum on the error surface in Fig. 2.6c. Using the entire set of calibrated parameters (Table 2.2), 2.0% of the 1283 glaciers were misclassified in the Juneau Icefield area (Table 2.3).

2.4.2 Validation

The calibrated parameters (Table 2.2) were ultimately applied to other regions of Alaska (Western Chugach Mountains, Western Alaska Range, Central Alaska Range, Eastern Alaska Range, Stikine Icefield, Fig. 2.5a) and southern Arctic Canada (Fig. 2.5b) to validate the algorithm. For the error assessment of each area, we created a set of visually checked reference outlines. The automatically derived outlines were then compared to the reference outlines, and errors were determined according to Equation (2.2).

As an example, Fig. 2.7 shows the individual glaciers for a subregion of the Western Alaska Range, indicating that glacier basins are properly separated. Overall, 1.9% out of 8121 glaciers were misclassified in Alaska's validation regions (Table 2.3). For southern Arctic Canada, 2.9% of the 7537 glaciers were misclassified.

There are five cases where the algorithm fails and leads to misclassified glaciers no matter the quality of DEM or glacier complex outlines. All these errors are considered in the error assessment (Table 2.3) and typical examples are illustrated in Fig. 2.8. In Fig. 2.8a, the algorithm incorrectly splits the glacier complex into two glaciers because the radii R

are too small and do not cover both flowsheds. The opposite is illustrated in Fig. 2.8b. Here the algorithm incorrectly merges two glaciers because R is too large and merges two flowsheds that should remain separate. Fig. 2.8c illustrates that glaciers ending within nunataks are not separated at all because the algorithm does not identify pour points along the borders of nunataks. The corresponding misclassifications contribute errors to the category 'merged incorrectly' in Table 2.3. In Fig. 2.8d, the algorithm fails to split the glacier complex into two glaciers because both glaciers have a shared accumulation area while, at the same time, the northern glacier reaches the southern glacier within the distance of buffer_1 . In this case, no flowsheds are calculated for the northern glacier individually as its flow is captured by the pour points of the southern glacier. These misclassifications also contribute errors to the category 'merged incorrectly'. Fig. 2.8e illustrates another reason why the algorithm may incorrectly split a glacier complex into too many glaciers. Columbia Glacier, shown in yellow, drains into multiple watersheds. If this occurs in the ablation area, such ice masses are generally not considered to constitute separate glaciers. The algorithm is not able to capture these cases because it treats all topographical divides equally, whether or not they are located in the glacier ablation areas.

Glacier separation also fails if small portions of glacier complexes reach over mountain ridges into different watersheds. In this case the algorithm correctly divides the complex into separate bodies, and sliver polygons are created. Although the problems with slivers are not technically an algorithm failure, we consider them in the error assessment. According to our validation, undetected slivers are the main contributor to the category 'split incorrectly' and thus an important contributor to the total number of errors (Table 2.3).

Manual intervention is finally required if the used DEM has poor quality. In this case, the derived topographic divides do not coincide with the true topographic divides. Consequences are most noticeable in flat accumulation areas, where small DEM errors have large impacts on the position of the ice divides (Fig. 2.9). Our error assessments and thus Table 2.3 exclude this error source because the errors are not related to a failure of the algorithm but rather to quality issues with the input data. Our assessments also exclude errors that occur due to flow divides that are not identical to the true topographic divides. As with errors due to inaccurate DEMs, flat accumulation areas are most susceptible to this last source of error.

2.5 Discussion

2.5.1 Algorithm performance

With success rates of $\sim 98\%$ (Alaska test areas) and $\sim 97\%$ (Arctic Canada test area), the algorithm shows a good overall performance (Table 2.3). The percentage of misclassified glaciers ranges between 1.2% (Western Alaska Range) and 2.9% (southern Arctic Canada). It is remarkable that two of the validation areas (Eastern and Western Alaska Range) have higher success rates than the calibration area, the Juneau Icefield. This is mainly because the Juneau Icefield contains a high number of complex geometries (such as glaciers branching in the ablation area) which lead to more misclassifications. Also, the DEM used in the Juneau Icefield area (ASTER GDEM2) has a relatively low quality. The lowest success rate, in Southern Arctic Canada, is most likely due to the prevalent complex glacier geometries, in conjunction with the lack of pronounced topographic relief. Moreover, DEM and glacier complex outlines for this region have the lowest quality of all the DEMs and outlines used in this study.

For most regions, the number of incorrectly split glaciers is disproportionately higher than the number of incorrectly merged glaciers (Table 2.3). At the same time, the median area of the incorrectly split glaciers is much lower than the median area of the incorrectly merged glaciers. This is consistent with our finding that undetected sliver polygons are one of the main contributors to the total error number.

We found that the algorithm fails to split glacier complexes into separate glaciers if pour points are not identified properly (failure of step 2, Fig. 2.2). This can occur if one glacier's tongue reaches another's within the distance of buffer 1, or if glaciers are located within nunataks along which the algorithm does not identify pour points. Although both cases are small contributors to the total error number, their elimination would further improve the performance of the algorithm.

A glacier complex is typically split into too many glaciers if the calculated flowsheds do not comply with the typical definition of a glacier (failure of steps 3 and 5). This occurs, for example, because small portions of glaciers often reach into neighboring watersheds, resulting in sliver polygons. The fact that slivers are the main contributor to the total number of errors indicates that our approach of using thresholds A_{sliver1} , A_{sliver2} and C_{sliver} is only partially successful in detecting sliver polygons. However, using A_{sliver2} in conjunction with C_{sliver} , we were able to reduce the number of slivers compared to the number

generated by using $A_{\text{sliver}1}$ only. We found that many slivers occur due to artifacts in DEM or glacier complex outlines. In the future, as DEM and glacier complex outlines continue to improve, we anticipate a reduction in the number of slivers.

A glacier complex is split into too many or too few glaciers if the flowsheds are merged incorrectly (failure of step 4, Fig. 2.2). This may occur if the derived pour points have atypical flow accumulation values. Cases of atypically low flow accumulation values and thus small R values are found for glaciers that have a high number of pour points. These cases are rare in our test areas, in part because the gutter significantly reduces the number of pour points. Nevertheless, the occasional failure of step 4 shows that our algorithm cannot deal correctly with the complex nature of all possible glacier shapes and topographies. At this stage, the algorithm needs a small amount of manual correction to obtain optimal results.

Significant manual intervention may be needed if the DEM used is of low quality. Consequences are most pronounced in flat accumulation areas, where small DEM errors have large impacts on the position of ice divides. While certain DEM products have sufficient quality to obtain reasonably accurate flowsheds, other DEM products should be used with care as input for our tool. The Shuttle Radar Topography Mission (SRTM) DEM, for example, produced reasonably accurate divides in our test areas. According to Frey et al. (2012), however, the use of the same DEM product is more problematic in other glacierized regions of the world. As the future will bring higher-quality DEMs, the influence of this error source will likely decrease. It is particularly promising that techniques such as InSAR yield good DEMs even in low-contrast glacier accumulation areas (Frey and Paul, 2012).

Our error assessment does not determine the algorithm's performance for different glacier types. However, it is plausible, and confirmed by visual inspections, that valley glaciers are most easily identifiable for our algorithm while ice caps pose the most challenges. Fig. 2.10 shows a mixed ice cap/valley glacier complex in southern Arctic Canada as separated by our algorithm. In their Fig. 7b, Svoboda and Paul (2009) provide a manually derived version of the same area. We compare the two solutions, although the DEMs and glacier complex outlines used in the two studies are not identical. While their manual approach derives four distinct glaciers overall, our approach derives seven glaciers. Svoboda and Paul (2009) combine glaciers 1, 2, and 3, which illustrates the fact that our algorithm divides ice caps into more sections than most manual approaches. The lobes

of the ice cap are sufficiently large for our algorithm to detect separate glaciers. Svoboda and Paul (2009) also combine our glaciers 5 and 6 (Fig. 2.10). Neither solution is ‘wrong’, however, they illustrate the subjectivity inherent in glacier separation and the difficulties of quantitatively assessing the performance of an automatic algorithm.

2.5.2 Transferability of parameters

Our method of applying one parameter set (Table 2.2) to entire regions proved to be robust for our test areas in Alaska and Arctic Canada. Although our test areas comprise a wide range of glacier geometries, more testing is required to determine transferability of parameters.

If optimization of parameters should become necessary for a new application area, six out of the ten parameters should be considered for adaptation: a , b , c , $A_{\text{sliver}1}$, $A_{\text{sliver}2}$ and C_{sliver} . However, algorithm success is not equally sensitive to all six parameters. Fig. 2.6, for example, illustrates that a small perturbation of b considerably changes the number of derived glaciers in our calibration area, while the same perturbation of a has a smaller influence. The parameter c has a limited influence if varied within a range (i.e., tens of meters) around the value specified in Table 2.2, because the R values of only a few large flowsheds are actually affected. Finally, it is plausible that the variation of the A_{sliver} and C_{sliver} parameters can significantly change the number of derived glaciers. Notably, C_{sliver} is sensitive to the shape of glacier complex outlines. Jagged outlines derived directly from raster data have lower compactness values compared to similar outlines with a smoothing filter applied. If outlines are derived entirely by hand, the level of digitized detail can also influence the compactness values. As a consequence, the same value for C_{sliver} can identify different numbers of sliver polygons only because different techniques have been used to derive the glacier complex outlines.

We recommend keeping the parameters DEM resolution, buffer1, buffer2, and L_{gutter} fixed, because they are strongly interrelated. L_{gutter} , for example, is optimized for the specified buffer widths. A change of the DEM resolution, would also implicitly require a recalibration of a and b , because these parameters are optimized for the spatial resolution of 40 m. Varying the spatial resolution changes the flow accumulation, F , at the pour points and thus affects the R values computed in Equation (2.1). We used a DEM resolution of 40 m because this cell spacing retains largescale relief features and allows for deriving reasonably accurate flowsheds. Even if the used DEM had excellent quality, a higher spatial

resolution would not significantly improve the quality of the glacier basins while the processing time increased considerably. As most large-scale DEMs used as input for this tool have a native resolution on the order of 40 m, any resampling to a higher spatial resolution would be impractical, leading to oversampling.

2.5.3 Error assessment

Our error assessment determined the number of errors semiautomatically. The results are reproducible provided reference outlines are available. Clearly, the availability of accurate reference outlines is the main limitation on our approach. In the present study, the reference outlines were obtained by visually scrutinizing outlines from the same algorithm that was eventually assessed using the checked reference outlines. As a consequence, the used reference outlines are not fully independent. The conducted visual checks are also partly subjective, as dividing glaciers can be subjective, despite the explicit definition of ‘a glacier’ in the literature (e.g., Racoviteanu et al., 2009). Given the large size of the test areas, errors may also be missed during visual checks. We aimed at reducing subjectivity by checking the reference outlines repeatedly and carefully. In the present study, we did not assess errors associated with technician interpretation. Ideally, however, future work should incorporate results from multiple interpreters.

We did not use available independent outlines because of the different techniques and standards used during derivation of these reference outlines. For example, Le Bris et al. (2011) published semi-automatically derived and manually checked outlines for the Western Chugach Mountains containing a high number of very small glaciers. These small glaciers occur because this study uses a different approach to address sliver polygons. Using their outlines for reference yields 350 misclassified glaciers (19.6% of the total number of glaciers), although larger glaciers are separated nearly identically. Clearly, the high number of errors does not reflect the general agreement between the two datasets.

Using the error area (i.e. the summed area of the misclassified glaciers), instead of the error number would be another way of quantifying the algorithm’s performance. However, we consider the error number more useful because it better reflects the amount of work required to adjust the dataset. The error area may be useful in the above case of the Western Chugach Mountains to show that the two datasets generally have a good agreement. In this particular case, the small overall area of the misclassified glaciers would reflect the good agreement. In general, however, the error area is not considered suit-

able to quantify the algorithm performance, mainly because it is very sensitive to outliers. One large incorrectly split glacier significantly increases the error area, not reflecting the amount of work required to adjust this error. In fact, misclassifications of large glaciers are particularly easy to identify through visual inspection and thus straightforward to repair.

Our error assessment excludes misclassifications due to DEM inaccuracies that cause derived topographic divides to be different from the true topographic divides. Although adjustments of these errors can be very time-consuming, we exclude these errors because they are not directly related to a failure of the algorithm. Moreover, a reproducible quantification of these errors would be difficult as the required adjustments involve a shift of glacier boundaries only, as opposed to the merging and splitting of entire glaciers required to adjust the errors included in our error assessment. Also, to obtain suitable reference divides, either a high-quality DEM or velocity fields would be required. To date, none of these data are available for our test areas.

2.5.4 Previous algorithms

Quantitative comparisons of our algorithm to previous algorithms are complicated by the fact that these algorithms are only briefly described as part of broader inventory studies. Moreover, none of the publications contain extended error assessments or examples of the raw tool output that could be compared to the output of our algorithm.

Manley (2008) published the first semi-automatic separation algorithm and applied it to the glacier complexes of the Eastern Alaska Range. His work, also published on the GLIMS website (http://glims.colorado.edu/tools/icedivide_algorithms), established ideas that have been used in more recent publications, including the algorithm presented here. To summarize, Manley (2008) uses a DEM to calculate the median elevation of each individual glacier complex. Every gridcell below the median glacier elevation is considered a pour point. The Manley (2008) algorithm uses a now superseded scripting language, and we therefore were unable to test it against our approach. However, based on our understanding of the method, we speculate that misclassifications would occur because pour points located above the median glacier elevation would be missed. Moreover, as the median glacier elevations of glacier complexes vary, the glaciers of neighboring complexes would be treated differently. For example, a tongue would be identified as such if it is part of a glacier complex that has a high median elevation. A similarly shaped tongue would be missed if it is part of another complex that has a lower median elevation. These potential

limitations suggest that other ways to determine pour points, for example, by identifying local elevation minima (Schiefer et al., 2008) or flow accumulation maxima (this study), may be more promising.

Schiefer et al. (2008) identify pour points by searching for local elevation minima along the outlines of glacier complexes. If the relief between pour points exceeds a predefined elevation threshold, they are considered to belong to separate glaciers. Schiefer et al. (2008) optimize the elevation threshold for their study area in British Columbia, western Canada, which is characterized by pronounced topography. Their 250 m threshold represents a compromise between a lower threshold that identifies multiple termini along undulating glacier tongues and a higher threshold that fails to detect smaller glaciers. Manual checks carried out within the present study suggest that the resulting glacier outlines are very sensitive to the choice of the elevation threshold. In addition, the DEM quality is important, as one erroneously high cell is sufficient to raise the relief above the threshold. We speculate that the performance of our approach may be less susceptible to local topography and DEM quality than the approach of Schiefer et al. (2008).

A third approach by Bolch et al. (2010) is built around a fully automated watershed function from the *ArcGIS* software package. This function determines pour points automatically and outputs the watersheds. In their study area in western Canada, Bolch et al. (2010) obtain best results by running this function not on the outlines of the glacier complexes directly, but on a buffer 1000–1500 m outside the outlines. This has the advantage that the derived basins are not linked to the glacier morphology for a given period of time, so they can be used for different time periods and glacier extents. However, the large buffer distance also implies that the derived basins can contain more than one glacier. Two studies that applied this algorithm in western Alaska (Le Bris et al., 2011) and in the western Himalaya (Frey et al., 2012) found that the algorithm can generate numerous artificial polygons that have to be merged manually. Our algorithm addresses these problems using L_{gutter} and P_{glac} , which should reduce the amount of manual intervention overall.

2.6 Conclusions

We have developed a new algorithm to separate glacier complexes into individual glaciers. The algorithm is based on hydrological modeling tools and identifies individual glaciers semi-automatically. Application of the algorithm to $>60,000 \text{ km}^2$ of ice in Alaska ($\sim 98\%$ success rate) and Arctic Canada ($\sim 97\%$ success rate) indicates that the method is robust,

requiring only a small number of manual corrections. Most misclassifications are due to sliver polygons, which not only occur due to failure of the algorithm, but also due to inaccuracies of the glacier complex outlines or DEMs. Future refinements of the present algorithm, together with improved DEMs and outlines, are anticipated to further reduce the number of misclassifications. However, given the complicated nature of possible glacier geometries and inaccuracies of DEMs and glacier complex outlines, it will remain challenging to develop a fully automatic approach.

Sophisticated algorithms to split glacier complexes into single glaciers are a crucial link between the derivation of glacier complexes (e.g., from remote sensing data) and the many applications that require individual glacier outlines as input (e.g., the compilation of glacier inventories). While there has been a wealth of research on both the automatization of glacier complex delineation and glaciological applications, research with regard to the actual glacier separation has been rare. Accordingly, glacier outlines have remained underived for many glacierized areas even though the corresponding glacier complex outlines are available. To help remedy this problem, our code is available for use as well as further development.

2.7 Acknowledgements

Thanks are due to J. Rich, S. Herreid and A. Gardner for providing outlines and DEMs. Constructive comments by H. Frey and two anonymous reviewers improved the manuscript. G. Vance and H. Jiskoot also provided helpful comments.

Support for this work was provided by NASA under the Cryosphere Sciences Program (grants NNH10Z1A001N, NNX11AF41G, NNX11A023G) and the US National Science Foundation (grant EAR-0943742).

Table 2.1. Test regions and their datasets. Parameters (Table 2.2) were derived for the region labeled 'C' (calibration), while the same parameters were then applied to the regions labeled 'V' (validation)

Region (C/V)	Area km ²	Glacier complex outlines		DEM		
		Technique	Source	Technique (native resolution)	Quality	Source
Juneau Icefield (C)	4686	Manual from Landsat	Herreid 2011, unpublished	Spaceborne-Photogramm. (80 m)	Fair	ASTER ² GDEM2, (NASA ³ , METI ⁴)
Western Alaska R. (V)	5803	Manual from IKONOS	Rich 2011, unpublished	Airborne-Photogramm. (40 m)	Fair	NED ⁵ , (USGS)
Central Alaska R. (V)	3818	Manual from Landsat	Herreid 2010, unpublished	Airborne-Photogramm. (40 m)	Fair	NED ⁵ , (USGS ¹)
Eastern Alaska R. (V)	2654	Manual from Landsat	Herreid 2010, unpublished	Airborne-Photogramm. (40 m)	Fair	NED ⁵ , (USGS ¹)
Western Chugach M. (V)	6001	Automatic (Landsat), manual corrections	Le Bris and others, 2011	Spaceborne-Photogramm. (40 m)	Good	SPOT ⁶ , (CNES ⁷)
Stikine Icefield (V)	5734	Manual from Landsat	Kienholz 2012, unpublished	Spaceborne-Radar (30 m)	Good	SRTM ⁸ (NASA ³)
Southern Arctic C. (V)	40,893	Maps, Landsat, manual corrections	CanVec, Gardner and others, 2012	Airborne-Photogramm. (150 m)	Fair	CDED ⁹

¹ US Geological Survey

² Advanced Spaceborne Thermal Emission and Reflection Radiometer

³ National Aeronautics and Space Administration

⁴ Japanese Ministry of Economy, Trade and Industry

⁵ National Elevation Dataset

⁶ Satellite Pour l'Observation de la Terre (courtesy of SPIRIT program 2008)

⁷ Centre National d'Etudes Spatiales

⁸ Shuttle Radar Topography Mission

⁹ Canadian Digital Elevation Data

Table 2.2. Calibrated parameters used in this study. Buffer1 is used to clip the DEM, and buffer2 locates the gutter. L_{gutter} is the terrain lowering along buffer2. a and b are the parameters used in Equation (2.1) to calculate R . The parameter c constrains R to a maximum size. A_{sliver1} is the threshold area below which a polygon is merged with the glacier with the longest shared boundary no matter the compactness value. A_{sliver2} is the threshold area below which a polygon is merged with the glacier with the longest shared boundary if the compactness lies below the threshold C_{sliver}

Parameter	Magnitude and Unit
DEM resolution	40 m
Buffer1	160 m
Buffer2	80 m
L_{gutter}	100 m
a	14.3 m
b	0.5
c	3500 m
A_{sliver1}	100,000 m ²
A_{sliver2}	200,000 m ²
C_{sliver}	0.5

Table 2.3. Total number of glaciers in the test regions and number/fraction of misclassified glaciers. The misclassified glaciers are attributed to the categories 'split incorrectly' and 'merged incorrectly' and the median areas are given for each category

Region (Calibration/Validation)	Total number	Split incorrectly (Median area, km ²)	Merged incorrectly (Median area, km ²)	Total misclassified (Fraction, %)
Juneau Icefield (C)	1283	17 (0.15)	9 (1.71)	26 (2.0)
Western Alaska Range (V)	2852	23 (0.2)	12 (4.58)	35 (1.2)
Central Alaska Range (V)	842	12 (0.14)	6 (1.25)	18 (2.1)
Eastern Alaska Range (V)	663	8 (0.21)	3 (1.73)	11 (1.7)
Western Chugach Mountains (V)	1787	20 (0.24)	23 (7.04)	43 (2.4)
Stikine Icefield (V)	1977	34 (0.24)	10 (5.88)	44 (2.2)
Southern Arctic Canada (V)	7537	148 (0.28)	73 (18.58)	221 (2.9)

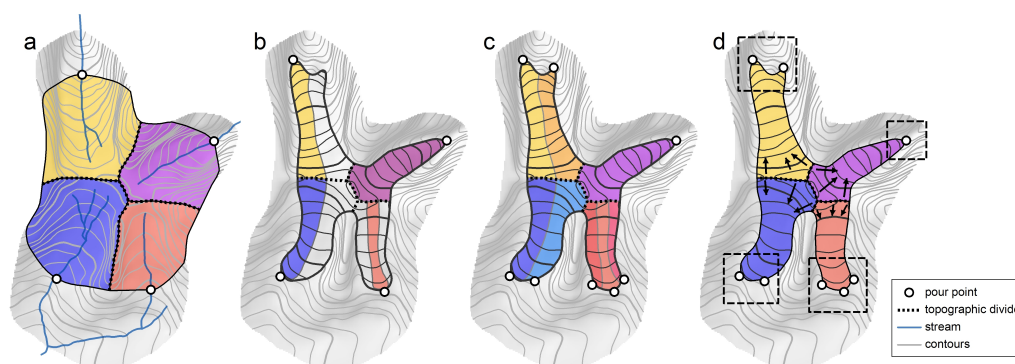


Figure 2.1. Principle of basin separation using hydrological modeling tools: (a) Watersheds (colored areas) calculated in unglacierized terrain using the lowest point of the valley cross section as a single pour point (black circles). (b) Flowsheds in glacierized terrain (colored areas) obtained if only the lowest-lying glacier gridcell is used as pour point. (c) Location of pour points and corresponding flowsheds necessary to capture the entire surface area of the glacier complex. (d) The same situation as in (c) but dashed boxes indicate which pour points belong to the same glacier. Black arrows mark the direction of ice flow.

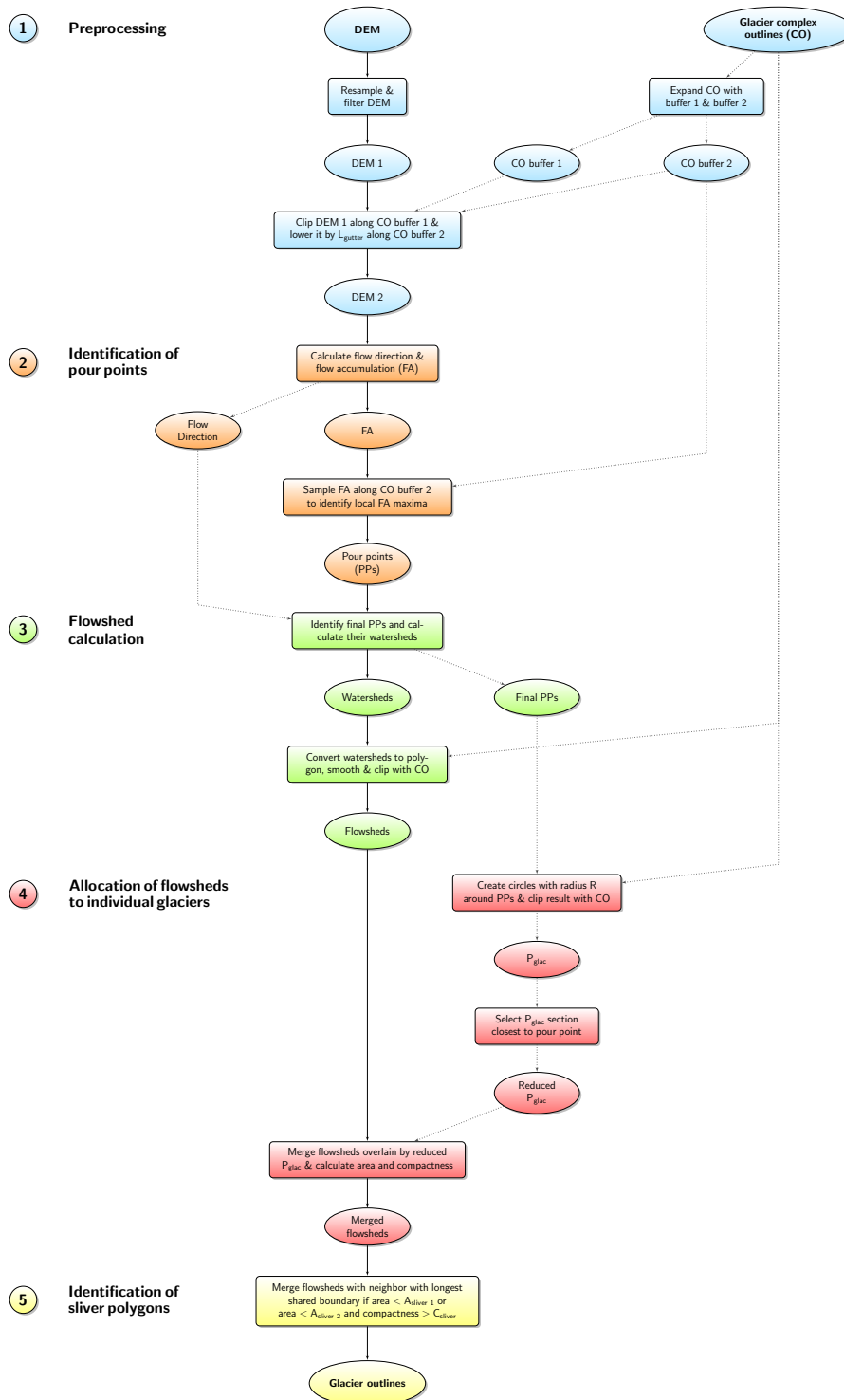


Figure 2.2. Diagram illustrating the conceptual workflow of the separation algorithm. Ovals represent input/output data while rectangles show the main operations. Solid arrows indicate the main progression, and dashed arrows show auxiliary steps.

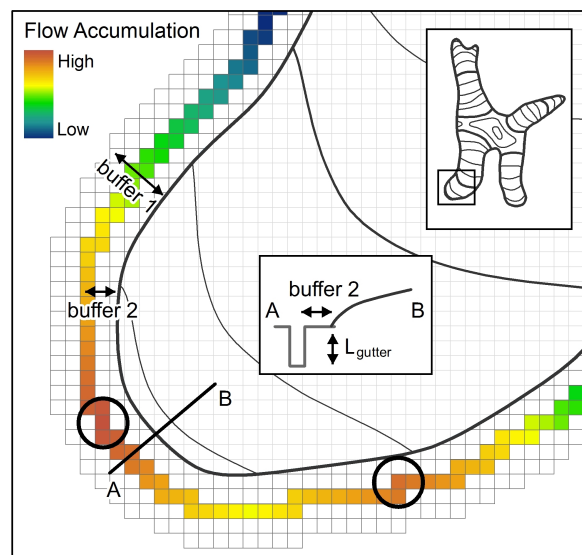


Figure 2.3. Example showing the DEM grid cells of a glacier terminus including the surrounding buffer region. Buffer1 is used to extract the DEM. Along buffer2, the grid is lowered artificially by the distance L_{gutter} to form a gutter. Colors indicate flow accumulation within the gutter. Circles mark pour points defined as gridcells with local flow accumulation maxima. 'A-B' is a cross-profile illustrated by the inset diagram, showing the cross-sectional geometry of the gutter.

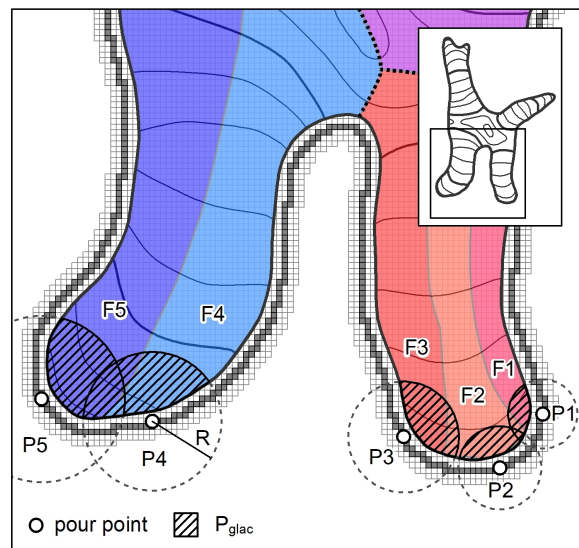


Figure 2.4. Location of pour points and corresponding flowsheds. Dashed circles indicate the radius R . The cross-hatched regions indicate the parts of the circles, P_{glac} , that are covered by glacier ice. When two or more flowsheds are overlain by a particular P_{glac} , those flowsheds are merged. For example, F1 and F2 are merged because they are overlain by P_{glac} of P1. P_{glac} of P3 overlaps F3 and F2 (F2 is already merged with F1 due to P1). P_{glac} of P4 overlaps F4 and F5 (the same is the case for P5), so F4 and F5 are also merged. Summarized, F1, F2, and F3 as well as F4 and F5 are merged, which is the targeted result shown in Fig. 2.1d.

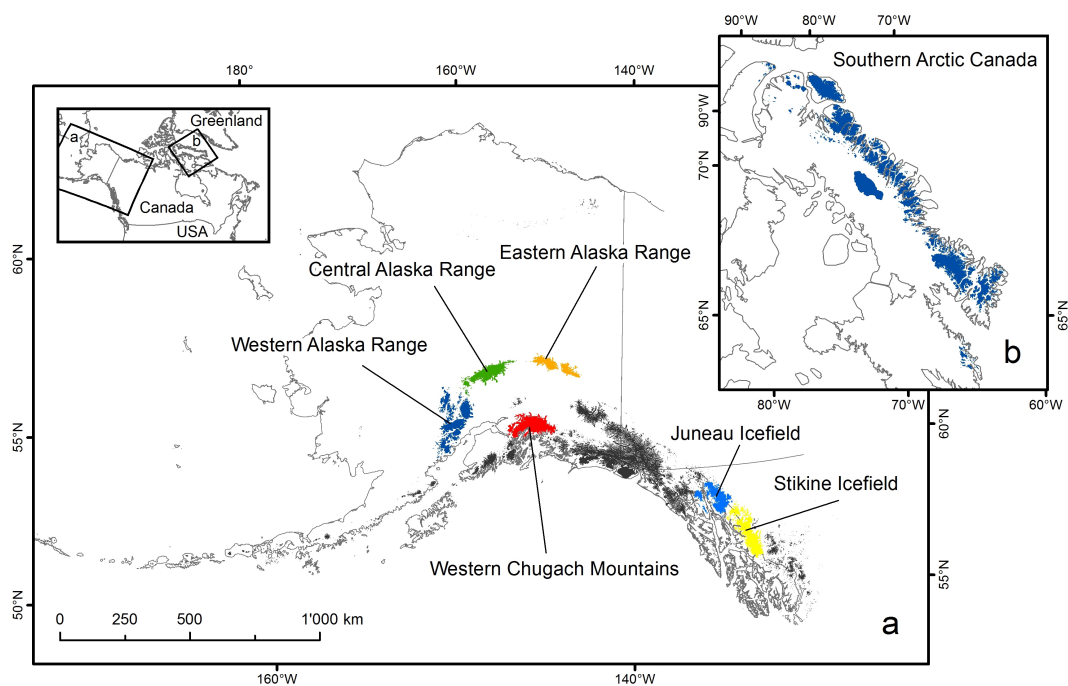


Figure 2.5. Location of glacier complexes to which the new algorithm was applied: (a) Alaska and (b) southern Arctic Canada. Both maps have the same scale.

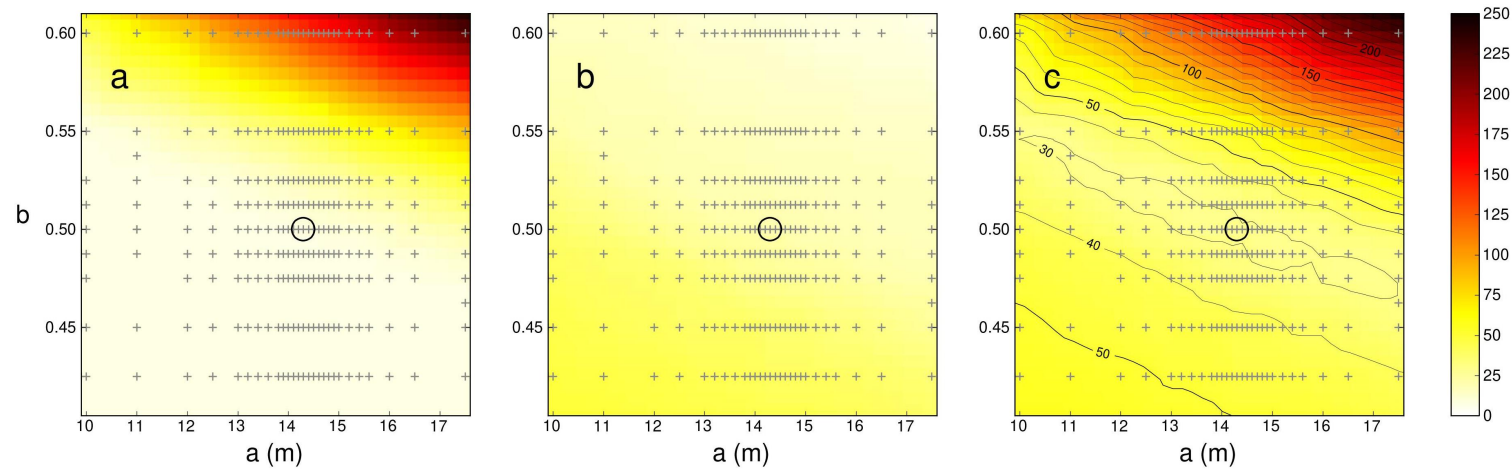


Figure 2.6. The number of misclassifications obtained in the Juneau Icefield test area as a function of the applied a and b values: (a) category 'merged incorrectly', (b) 'split incorrectly' and (c) 'total misclassified'. Crosses indicate individual test runs. Error surfaces are interpolated from the number of errors at each cross. Contours are added in (c) as an additional reference. The black circles show the combination of parameters a and b (14.3 m and 0.5) that yielded a minimum of 26 errors.

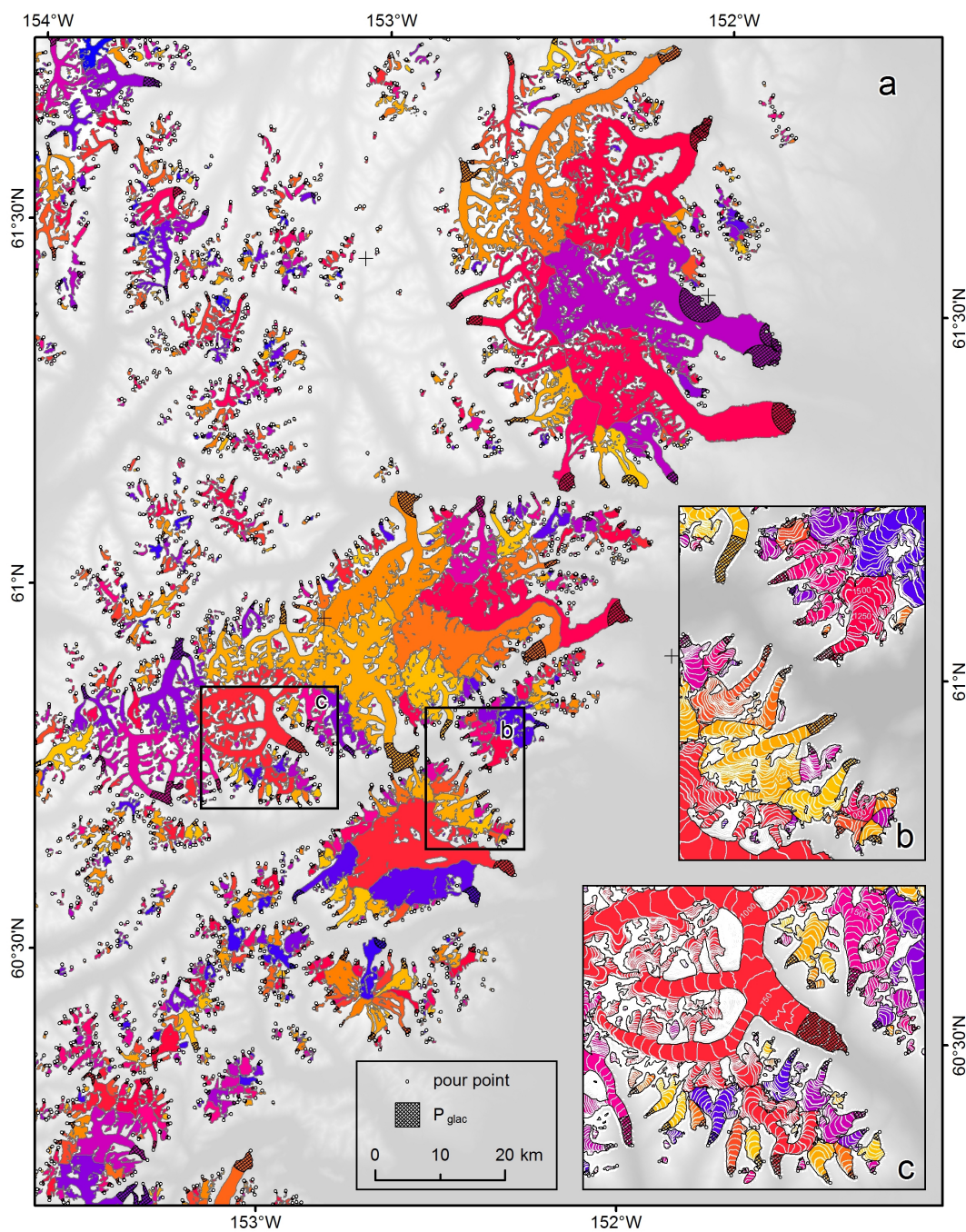


Figure 2.7. Color-coded glacier outlines automatically derived for a subregion of the Western Alaska Range. The white dots are the pour points. Cross-hatched polygons indicate the P_{glac} used to merge separate flowsheds. The enlarged insets (b) and (c) have white 50 m contours added that can be checked against the glacier outlines for validation. See Table 2.1 for sources of the original glacier complex outlines.

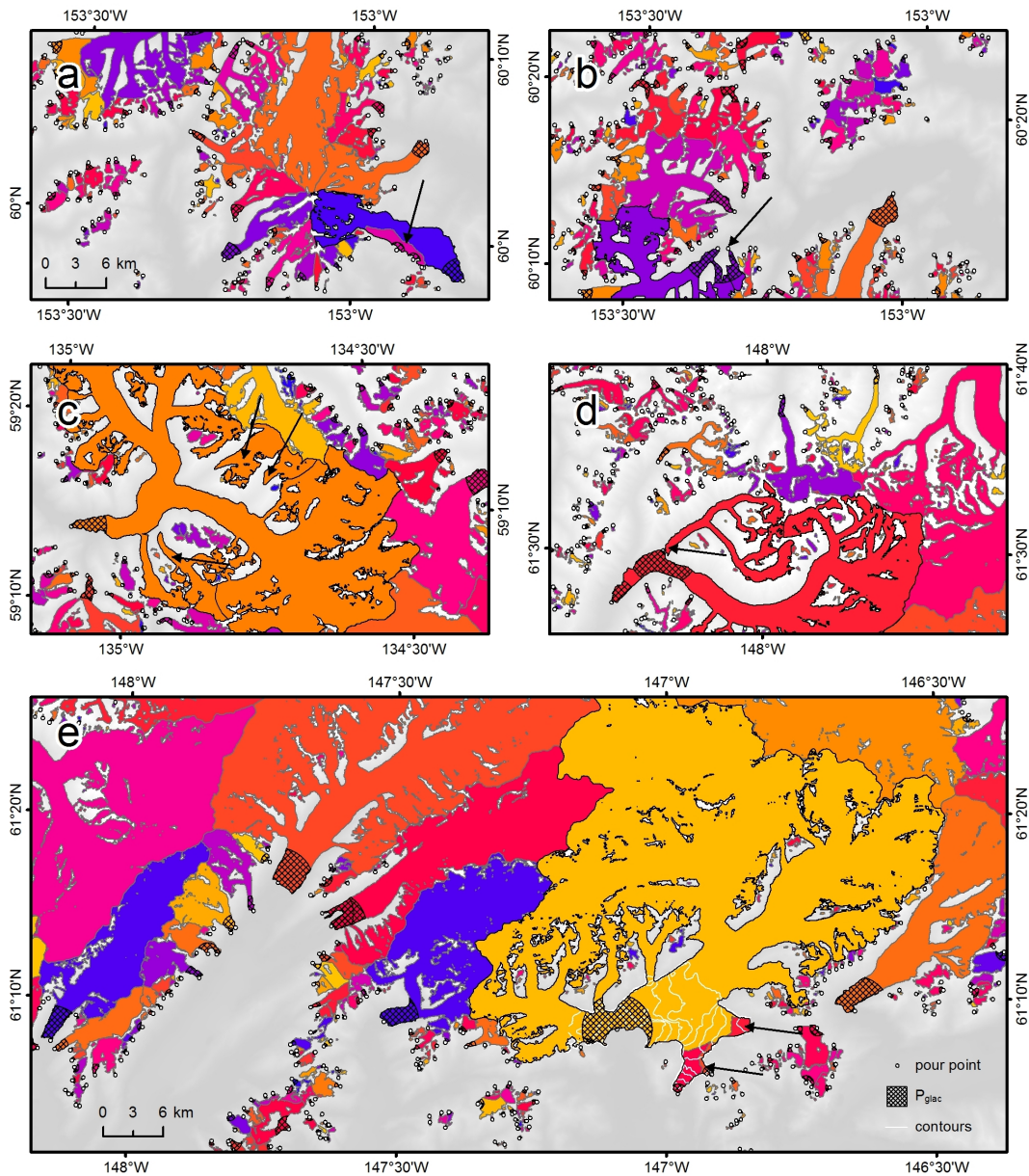


Figure 2.8. Glacier basins (color-coded) for selected subregions of the Eastern Alaska Range (a–b), the Juneau Icefield (c), and the Western Chugach Mountains (d–e). The arrows indicate cases of misclassification. White dots indicate pour points, and the crosshatched polygons are the P_{glac} used to merge the flowsheds of individual glaciers. The black polygons are manually adjusted glacier polygons from the reference glacier outlines. The white 50 m contours in (e) illustrate the topographical divide within the ablation area of Columbia Glacier. Table 2.1 states the sources of the original glacier complex outlines. All the maps have the same scale.

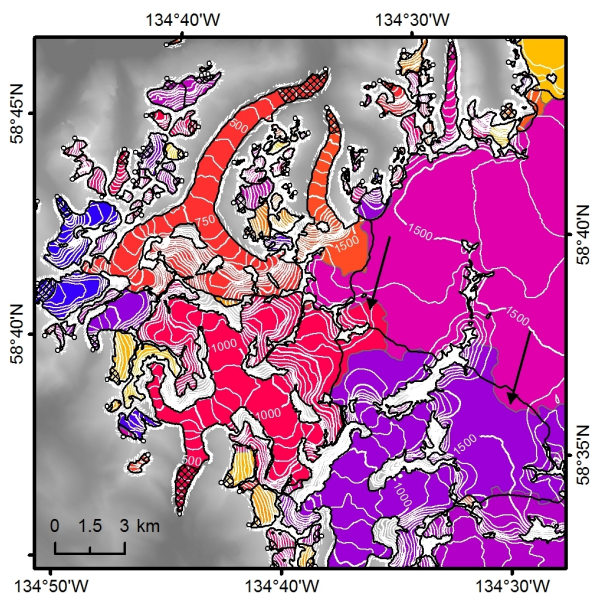


Figure 2.9. Failed automatic glacier separations in the Juneau Icefield area. Colors indicate individual glaciers separated by our algorithm using the ASTER GDEM2 while black lines define the glaciers using the same algorithm with a more reliable DEM (SRTM). Large discrepancies occur in the eastern part of the domain (annotated by arrows) due to the poor quality of the ASTER GDEM2 in this part of the accumulation area.

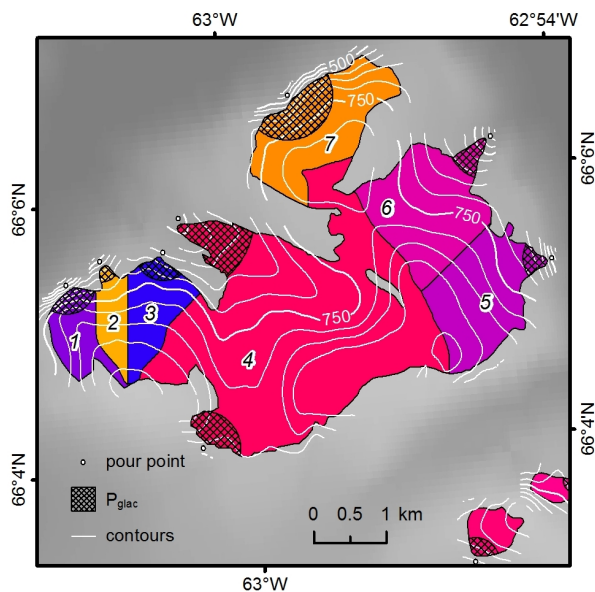


Figure 2.10. Glacier separation of a mixed ice cap/valley glacier complex in southern Arctic Canada. This figure corresponds to Fig. 7b in Svoboda and Paul (2009). In their manual solution, the glaciers annotated with 1, 2, and 3 as well as 5 and 6 are merged.

References

- Allen, T. (1998). Topographic context of glaciers and perennial snowfields, glacier national park, montana. *Geomorphology* 21(3), 207–216.
- Bahr, D., M. Meier, and S. Peckham (1997). The physical basis of glacier volume-area scaling. *Journal of Geophysical Research* 102(B9), 20355–20362.
- Beedle, M., M. Dyurgerov, W. Tangborn, S. Khalsa, C. Helm, B. Raup, R. Armstrong, R. Barry, et al. (2008). Improving estimation of glacier volume change: a GLIMS case study of Bering Glacier System, Alaska. *The Cryosphere* 2(1), 33–51.
- Bolch, T., B. Menounos, and R. Wheate (2010). Landsat-based inventory of glaciers in western canada, 1985-2005. *Remote Sensing of Environment* 114(1), 127–137.
- Frey, H. and F. Paul (2012). On the suitability of the srtm dem and aster gdem for the compilation of topographic parameters in glacier inventories. *International Journal of Applied Earth Observation and Geoinformation* 18, 480–490.
- Frey, H., F. Paul, and T. Strozzi (2012). Compilation of a glacier inventory for the western himalayas from satellite data: methods, challenges, and results. *Remote Sensing of Environment* 124, 832–843.
- Gardner, A., G. Moholdt, A. Arendt, and B. Wouters (2012). Long-term contributions of baffin and bylot island glaciers to sea level rise: an integrated approach using airborne and satellite laser altimetry, stereoscopic imagery and satellite gravimetry. *The Cryosphere Discussions* 6, 1563–1610.
- Huss, M. and D. Farinotti (2012). Distributed ice thickness and volume of all glaciers around the globe. *Journal of Geophysical Research* 117(F4), F04010.
- Kargel, J., M. Abrams, M. Bishop, A. Bush, G. Hamilton, H. Jiskoot, A. Kääb, H. Kieffer, E. Lee, F. Paul, et al. (2005). Multispectral imaging contributions to global land ice measurements from space. *Remote Sensing of Environment* 99(1), 187–219.
- Le Bris, R., F. Paul, H. Frey, and T. Bolch (2011). A new satellite-derived glacier inventory for Western Alaska. *Annals of Glaciology* 52(59), 135–143.

- Linsbauer, A., F. Paul, and W. Haeberli (2012). Modeling glacier thickness distribution and bed topography over entire mountain ranges with glabtop: Application of a fast and robust approach. *Journal of Geophysical Research* 117(F3), F03007.
- Manley, W. (2008). Geospatial inventory and analysis of glaciers: A case study for the eastern Alaska Range. In R. S. William and J. G. Ferrigno (Eds.), *Satellite image atlas of glaciers of the world*. U.S. Geological Survey Professional Paper 1386-E, 525 pp.
- Paul, F., C. Huggel, and A. Kääb (2004). Combining satellite multispectral image data and a digital elevation model for mapping debris-covered glaciers. *Remote Sensing of Environment* 89(4), 510–518.
- Paul, F., A. Kääb, M. Maisch, T. Kellenberger, and W. Haeberli (2002). The new remote sensing derived Swiss glacier inventory: I. Methods. *Annals of Glaciology* 34, 355–361.
- Racoviteanu, A., F. Paul, B. Raup, S. Khalsa, and R. Armstrong (2009). Challenges and recommendations in mapping of glacier parameters from space: results of the 2008 global land ice measurements from space (glims) workshop, boulder, colorado, usa. *Annals of Glaciology* 50(53), 53–69.
- Radić, V. and R. Hock (2010). Regional and global volumes of glaciers derived from statistical upscaling of glacier inventory data. *Journal of Geophysical Research* 115, F01010.
- Radić, V. and R. Hock (2011). Regionally differentiated contribution of mountain glaciers and ice caps to future sea-level rise. *Nature Geoscience* 4(2), 91–94.
- Raup, B. and S. J. S. Khalsa (2007). *GLIMS Analysis Tutorial*. GLIMS.
- Schiefer, E., B. Menounos, and R. Wheate (2008). An inventory and morphometric analysis of British Columbia glaciers, Canada. *Journal of Glaciology* 54(186), 551–560.
- Svoboda, F. and F. Paul (2009). A new glacier inventory on southern baffin island, canada, from aster data: I. applied methods, challenges and solutions. *Annals of Glaciology* 50(53), 11–21.

Chapter 3

A new method for deriving glacier centerlines applied to glaciers in Alaska and northwest Canada¹

3.1 Abstract

This study presents a new method to derive centerlines for the main branches and major tributaries of a set of glaciers, requiring glacier outlines and a digital elevation model (DEM) as input. The method relies on a ‘cost grid – least cost route approach’ that comprises three main steps. First, termini and heads are identified for every glacier. Second, centerlines are derived by calculating the least cost route on a previously established cost grid. Third, the centerlines are split into branches and a branch order is allocated. Application to 21,720 glaciers in Alaska and northwest Canada (Yukon, British Columbia) yields 41,860 centerlines. The algorithm performs robustly, requiring no manual adjustments for 87.8% of the glaciers. Manual adjustments are required primarily to correct the locations of glacier heads (5.5% corrected) and termini (3.5% corrected). With corrected heads and termini, only 1.4% of the derived centerlines need edits. A comparison of the lengths from a hydrological approach to the lengths from our longest centerlines reveals considerable variation. Although the average length ratio is close to unity, only ~50% of the 21,720 glaciers have the two lengths within 10% of each other. A second comparison shows that our centerline lengths between lowest and highest glacier elevations compare well to our longest centerline lengths. For >70% of the 4350 glaciers with two or more branches, the two lengths are within 5% of each other. Our final product can be used for calculating glacier length, conducting length change analyses, topological analyses, or flowline modeling.

3.2 Introduction

Glacier centerlines are a crucial input for many glaciological applications. For example, centerlines are important for determining glacier length or thickness changes over time (Leclercq et al., 2012; Nuth et al., 2013), analyzing velocity fields (Heid and Käab, 2012; Melkonian et al., 2013), estimating glacier volumes (Li et al., 2012; Linsbauer et al., 2012), and one-dimensional modeling of glaciers (Oerlemans, 1997a; Sugiyama et al., 2007). Also, glacier length, derived from centerlines, is an important parameter for glacier inventories (Paul et al., 2009).

¹Kienholz, C., J. L. Rich, A. A. Arendt, and R. Hock (2013). *The Cryosphere Discussions* 7 (5), 5189–5229.

So far, most of the above applications have relied on labor-intensive manual digitization of centerlines. The few studies that derive centerlines fully automatically use a hydrological approach and/or derive only one centerline per glacier (Schiefer et al., 2008; Le Bris and Paul, 2013). Here, we present a new algorithm that allows for deriving multiple centerlines per glacier based on a digital elevation model (DEM) and outlines of individual glaciers. Moreover, this algorithm splits the centerlines into branches and classifies them according to a geometry order. The approach is tested on all glaciers in Alaska and adjacent Canada with an area $>0.1 \text{ km}^2$, corresponding to 21,720 out of 26,950 glaciers. We carry out a quality analysis by visual inspection of the centerlines, and compare the derived lengths to the lengths obtained from alternative approaches.

3.3 Previous work

The automatic derivation of glacier centerlines and thereof retrieved glacier length is considered challenging (Paul et al., 2009, Le Bris and Paul, 2013). Consequently, only a few automated approaches have been proposed so far (Schiefer et al., 2008; Le Bris and Paul, 2013) and often, centerlines have been digitized manually even for large-scale studies.

In their large-scale study, Schiefer et al. (2008) applied an automated approach to all British Columbia glaciers that is based on hydrology tools. For each glacier, this approach derives one line that represents the maximum flow path that water would take over the glacier surface. Schiefer et al. (2008) find that these lengths are 10-15% longer than distances measured along actual centerlines. Because lower glacier areas (\sim ablation areas) are typically convex in cross-section, their flow paths are deflected toward the glacier margins, which leads to length measurements that are systematically too long in these cases. While systematically biased lengths in a glacier inventory can be corrected for, the actual lines need major manual corrections before they can be used in glaciological applications such as flowline modeling. Therefore, Paul et al. (2009) suggest the use of the above automated algorithm in the concave (i.e., higher) part of the glacier, combined with manual digitization in the convex (lower) part of the glacier.

Le Bris and Paul (2013) present an alternative method for calculating glacier centerlines based on a so-called 'glacier axis' concept, which derives one centerline per glacier between the highest and the lowest glacier elevation. Le Bris and Paul (2013) first establish a line (the 'axis') between the highest and the lowest glacier point, which is then used to compute center points for the glacier branches. These center points are connected,

starting from the the highest glacier elevation and following certain rules (e.g., ‘always go downward’, ‘do not cross outlines’). Smoothing of the resulting curve leads to the final centerline. The algorithm is applicable to most glacier geometries, yielding results similar to manual approaches (Le Bris and Paul, 2013). A limitation of their approach is the fact that the derived centerline between the highest and lowest glacier elevation does not necessarily represent the longest glacier centerline or the centerline of the main branch, either one of them often required in glaciological applications. For example, for glacier inventories, it is recommended to measure glacier length along the longest centerline, or, alternatively, to average the lengths of all glacier branches (Paul et al., 2009).

3.4 Test site and data

Our algorithm is tested on glaciers located in Alaska and adjacent Canada (Fig. 3.1a). For brevity, we hereafter refer to these glaciers as Alaska glaciers. From the complete Alaska glacier inventory (Arendt et al., 2013), we extract all glaciers with a minimal area threshold of $>0.1 \text{ km}^2$, thus eliminating small glacierets and possible perennial snowfields. This results in 21,720 glaciers with 86,400 km^2 of ice total, which accounts for more than 99% of the area of the complete Alaska inventory.

The Alaska glacier inventory comprises glacier outlines derived from satellite imagery taken between ~ 2000 and 2012. The outlines used herein either stem from manual digitization at the University of Alaska Fairbanks or from automated band ratioing followed by visual quality checks and manual corrections (Bolch et al., 2010; Le Bris et al., 2011, Fig. 3.1a).

Four DEM products are combined to create a continuous 60 m DEM consistent with the time-span covered by the glacier outlines (Fig. 3.1b). South of 60N, we rely on the Shuttle Radar Topography Mission (SRTM) DEM (<http://www2.jpl.nasa.gov/srtm>, access: 25 July 2013), taken in February 2000 (Farr et al., 2007). Over Alaska, the SRTM DEM has a native spatial resolution of 30 m, while the resolution is 90 m over Canada. North of 60N, we use a high quality DEM derived from airborne Interferometric Synthetic Aperture Radar (IFSAR) data obtained in 2010 (Geographic Information Network of Alaska GINA, <http://ifsar.gina.alaska.edu>, access: 25 July 2013). For areas not covered by the IFSAR DEM, we use DEMs derived from data from the High Resolution Stereo (HRS) imaging instrument onboard the Système Pour l’Observation de la Terre (SPOT) satellite taken within the scope of the SPIRIT program (time span 2007–2008, Korona et al., 2009) and the

Advanced Spaceborne Thermal Emission and Reflection Radiometer (ASTER) instrument onboard the Terra satellite (ASTER GDEM2, time span 2000–2011, Tachikawa et al., 2011, <http://asterweb.jpl.nasa.gov/gdem>, access: 25 July 2013). The individual DEM tiles are merged into one dataset giving priority to the highest quality DEM available for each area. While the used DEMs represent roughly the same time span, the goals and scopes of the individual campaigns are different, which becomes apparent in the contrasting quality of the DEMs. For example, the GDEM has nearly global coverage, but limited quality, while the IFSAR DEM is of high quality, but only available for parts of Alaska.

3.5 Method

Our goal is to design an algorithm that (1) creates centerlines for the main glacier branches as well as major tributaries, (2) yields a quality comparable to a manual approach, and (3) requires minimal data and manual intervention. It would be desirable to derive centerlines that represent actual flowlines (i.e., ice trajectories), however, this would require coherent velocity fields without gaps. While corresponding algorithms are applied for single glaciers (e.g., McNabb et al., 2012), stringent velocity data requirements make large-scale applications difficult. Here, we aim at obtaining centerlines that are close to flowlines by only using glacier outlines and a DEM as input. Such centerlines differ from flowlines mostly in areas, where centerlines from different glacier branches converge. Actual flowlines would not converge completely, but run roughly in parallel to the glacier terminus, as illustrated, for example, by Farinotti et al. (2009). Although not entirely consistent with real flowlines, centerlines are used for modeling purposes (e.g., Oerlemans, 1997b; Leclercq et al., 2012). They can also be used for applications that generally have lower requirements than does modeling (e.g., determining length changes, deriving glacier length for inventories).

Here, we apply a method that we call a ‘cost grid – least cost route approach’. The workflow consists of three main steps that are implemented using the Python™ programming language. The first step comprises the identification of glacier termini and glacier heads. The second step encompasses the calculation of a cost grid, followed by determining and optimizing the least cost route to derive the glacier centerlines. In the third step, these centerlines are split into branches and a geometry order is introduced. Because the three steps are associated with different uncertainties, we have separate modules for each step of the algorithm.

3.5.1 Step 1 – Identification of glacier heads and termini

In the first step, we identify glacier heads and termini by applying a search algorithm based on the DEM and glacier outline. We aim to derive one terminus per glacier and one head for each major glacier branch. The centerlines eventually run from each glacier head to the terminus.

3.5.1.1 Glacier terminus

A natural way of identifying the glacier terminus is by extracting the lowest glacier cell (e.g., Le Bris and Paul, 2013). To better constrain our lowest point to the actual terminus, we apply the corresponding query on a low-pass filtered and ‘filled’ DEM. ‘Filling’ refers to removing depressions within the DEM that could hamper the identification of the actual glacier terminus. We consider filling and filtering as most important for large receding glaciers, ending in flat terrain, that are generally characterized by a rough surface with numerous depressions.

Fig. 3.2a shows the glacier terminus as automatically obtained for Gilkey Glacier, an outlet glacier of the Juneau Icefield located in southeast Alaska.

3.5.1.2 Glacier heads

Since we aim to derive centerlines of all major glacier branches, we need to identify heads for each of these branches. A three-step procedure is adopted to identify these heads (Fig. 3.3). First we identify local elevation maxima along the glacier outlines. Our algorithm samples the DEM in predefined steps (100 m) along the glacier outline (including nunataks) and then compares each sampled elevation to its neighboring points along the outline. A possible glacier head is identified if the local point is higher than its neighbors (five neighbors in each direction, Fig. 3.3a) and if the point is higher than the lowest one third of the elevation distribution of all the sampled points of the corresponding glacier (Fig. 3.3b). We apply the second criterion since glacier heads are typically located at higher elevations. We also want to avoid assigning centerlines to low-lying minor tributaries.

Given the irregular shapes of typical glacier outlines, the workflow above can result in multiple heads per glacier branch. To remove multiple heads per branch, we introduce a minimum linear distance r (m) that the derived heads must be apart. Since larger glaciers tend to have wider basins, we define r as a function of glacier area S (m^2) according to

Equation 3.1:

$$r = \begin{cases} q_1 \cdot S + q_2 & : r \leq r_{\max} \\ r_{\max} & : r > r_{\max} \end{cases} \quad (3.1)$$

q_1 , q_2 and r_{\max} are constants given in Table 3.1. In case one or more heads are within r , we only retain the highest head and erase all others (Fig. 3.3c). If two heads are apart by a distance less than r but separated by a nunatak, both heads are retained. A nunatak is identified if the circle defined by r splits the glacierized area into two or more parts (Fig. 3.3d).

In case no head is identified using the above steps, which can be the case for small glaciers, we identify the highest glacier elevation as the glacier head. In case of Gilkey Glacier, 77 heads are identified (Fig. 3.2a).

3.5.2 Step 2 – Establishment of cost grid and determination of least cost route

This step establishes a cost or penalty grid (here used as synonyms) with high values at the glacier edge and in upper reaches of the glacier. The penalty values decrease towards the glacier center as well as towards lower elevations. The least cost route from a glacier head to the glacier terminus yields the centerline.

3.5.2.1 Cost/penalty grid and route cost

First, we create a penalty grid with $10 \text{ m} \times 10 \text{ m}$ cell size according to Equation 3.2. We choose this small cell size to obtain a detailed representation of the glacier outlines in the gridded map. A larger cell size would yield a coarser glacier grid omitting small-scale features such as small nunataks. The penalty value p_i of each grid cell i within the glacier is computed by

$$p_i = \left(\frac{\max(d) - d_i}{\max(d)} \cdot f_1 \right)^a + \left(\frac{z_i - \min(z)}{\max(z) - \min(z)} \cdot f_2 \right)^b \quad (3.2)$$

d_i is the Euclidean distance from cell i to the closest glacier edge and z_i is the corresponding elevation. $\max(d)$, $\max(z)$ and $\min(z)$ are the glacier's maximum Euclidean distance, maximum elevation, and minimum elevation, respectively. The 'stretching' factors

f_1 and f_2 and the ‘weighting’ exponents a and b obtained for our study area are given in Table 3.1.

The first term $\frac{\max(d)-d_i}{\max(d)}$ normalizes d_i to the maximum Euclidean distance found on the glacier, and leads to a Euclidean penalty contribution that ranges between zero and one (i.e., zero at the cell(s) with $\max(d)$ and one along the glacier edge). By multiplying the term with f_1 , we stretch the normalized values to a range between zero and f_1 . The second term $\frac{z_i-\min(z)}{\max(z)-\min(z)}$ normalizes the elevation of each grid cell to the elevation range of the entire glacier, and yields an elevation penalty contribution that is zero at the glacier terminus, where $z = \min(z)$, and one at the highest glacier point, where $z = \max(z)$. f_2 stretches these values to a range between zero and f_2 . While the first term tends to force the least-cost route to the glacier center, the second term tends to force it downslope. The exponents a and b control the weight each of these terms have. The normalization in Equation 3.2 is implemented to make the same a and b exponents better transferable to glaciers of different size and geometry.

f_1 and f_2 stretch the normalized values back to actual glacier dimensions. Both factors are derived from Chedotlotha Glacier, a medium sized glacier located in the Alaska Range that was used to calibrate the initial a and b exponents. As we applied an unnormalized version of Equation 3.2 to calibrate a and b , that is, $p_i = (\max(d) - d_i)^a + (z_i - \min(z))^b$, f_1 (1000, equivalent to $\max(d)_{\text{Chedot.}}$) and f_2 (3000, equivalent to $\max(z)_{\text{Chedot.}} - \min(z)_{\text{Chedot.}}$) are necessary to use these initially calibrated a and b values in the normalized Equation 3.2.

To obtain plausible centerlines, a strong increase in the penalty values is required close to the glacier boundary and at higher glacier elevations. High Euclidean distance-induced penalty values at the glacier boundary are crucial to prevent centerlines from reaching too close to the glacier edge, which would not match the expected course of flowlines. A strong elevation-induced penalty gradient at higher glacier altitudes is important to ensure that centerlines choose the correct branch from the start. By using a and b as exponentials and not as coefficients, we do obtain the highest penalty gradients close to the glacier edges and at high glacier elevations.

Fig. 3.4a shows the initial cost grid obtained for Gilkey Glacier. The first part of Equation 3.2 is dominating (penalties decrease strongly towards the branch centers), while the second part of the equation has a lower effect.

Using the cost grid obtained from Equation 3.2, we calculate the least cost route from each head to the glacier terminus, which corresponds to the path with the minimum route

cost. The route cost c is defined by the sum of the penalty values p_i between the glacier head and the terminus,

$$c = \sum_{i=1}^I p_i \quad (3.3)$$

where I is the total number of cells crossed from the glacier head to the glacier terminus. The optimal path is not necessarily the shortest path (minimal I), because the penalty values p_i are not constant. For example, given a meandering glacier, the shortest route is expensive, because it crosses cells with very high penalty values at the edge of the glacier. Instead, it is cheapest to stay near the center of the glacier. Although this route crosses more cells (higher I), the resulting sum of penalties is smaller as the penalty values (p_i) are considerably smaller near the glacier center.

In a next step, we convert the above least cost route, which is obtained as a raster dataset, to a vector format. We then smooth the corresponding curve using a standard Polynomial Approximation with Exponential Kernel (PEAK) algorithm. This algorithm calculates a smoothed centerline by applying a weighted average on the vertices of a moving line-subsegment. A longer subsegment leads to more smoothing. We define the length of the subsegment, l (m), for every glacier individually, by

$$l = \begin{cases} u_1 \cdot S + u_2 & : l \leq l_{\max} \\ l_{\max} & : l > l_{\max} \end{cases} \quad (3.4)$$

where S is the glacier area in m^2 . The constants u_1 , u_2 and l_{\max} are given in Table 3.1. l is increased as a function of the glacier area to account for the wider branches and the smooth course of the centerline typical for larger glaciers.

For simple glacier geometries, the first term alone in Equation 3.2 already creates plausible centerlines; however, for more complex geometries, the resulting centerlines can ‘flow’ unreasonably upslope and choose a wrong route. Because elevation (or slope) is neglected in the first term, the centerlines stick to the glacier center regardless of the topography. To remedy this problem, the elevation-dependent term is essential in Equation 3.2. The elevation-dependent term also forms the basis for the optimization step introduced next.

3.5.2.2 Optimization

During the optimization we aim to find a combination of a and b values (Equation 3.2) that provides the most plausible solution for each centerline. Our approach is based on the following considerations: if a narrow and a wide basin are connected in their upper reaches, centerlines will typically flow through the wide basin, because the penalty values are smaller in the center of the wide basin compared to the center of the narrow basin. This is illustrated in Fig. 3.4a, where wide basins have lower penalty values in the center than narrow basins. In some cases, the centerlines may flow a significant distance upslope and make a major detour to reach a wider basin, and still have minimum route cost. In these cases, the low penalty values in the center of the reached wide basin overcompensate for the additional penalties due to the detour. This implies that the weight of the second term of Equation 3.2 is too low compared to the weight of the first term. Incrementally increasing the second part of Equation 3.2 will eventually force the centerline to take a route that is shorter and typically characterized by less upslope flow. Ideally, this is the correct centerline.

To obtain the initial centerlines, we apply a and b values of 4.25 and 3.5, respectively (Table 3.1), as derived from tests in the Alaska Range. During the optimization, we keep a constant and raise b in discrete steps Δb (0.1 per iteration, Table 3.1), thereby increasing the weight of the elevation component in Equation 3.2. Not all centerlines require an optimization, and in case centerlines require optimization, b can not be increased infinitely, as this leads to a loss of the expected ‘natural’ course of the centerline. Fig. 3.4a illustrates this on Gilkey Glacier, where most initial centerlines have plausible routes. Only the centerlines marked by circles have implausible routes with major upslope flow and thus clearly need optimization. Figures 3.4b-d show that an increase of b improves the lines in need of optimization (i.e., the implausible centerlines circled in Fig. 3.4a take the correct route in Fig. 3.4b), while it may diminish the quality of the remaining centerlines due to the higher weight of the elevation term, which forces centerlines to ‘cut corners’ instead of sticking to the glacier center. Accordingly, a criterion is needed to determine whether optimization is necessary, and in case it is, to decide when to terminate the optimization. For this purpose, we sample the DEM along each centerline and determine the total elevation increase in m (Δz_{up} , Equation 3.5, Fig. 3.5) and the maximum number of samples with continuously increasing elevation (n_{up} , Equation 3.6, Fig. 3.5).

$$\Delta z_{\text{up}} = \sum_{i=1}^I \Delta z_{\text{up},i} \quad (3.5)$$

$$n_{\text{up}} = \max(n_{\text{up},i}) \quad (3.6)$$

I is the total number of individual centerline sections with upslope flow.

Δz_{up} and n_{up} are used to calculate the iteration threshold m (Equation 3.7). Comparison of m to the number of accomplished iterations determines whether farther iterations are carried out.

$$m = \begin{cases} n_{\text{up}} + j_1 \cdot \Delta z_{\text{up}}^{j_2} & : m \leq m_{\text{max}} \\ m_{\text{max}} & : m > m_{\text{max}} \end{cases} \quad (3.7)$$

j_1 , j_2 and m_{max} are given in Table 3.1. Equation 3.7 mimicks our concept of having a high number of iterations if a large n_{up} coincides with a high Δz_{up} ('worst case', e.g., C-1 in Fig. 3.6a), as this is a very strong indicator for a wrong course of the preliminary centerline. If both n_{up} and Δz_{up} are zero, m is also zero as we assume that the preliminary centerline already takes the correct branch. If a high Δz_{up} occurs in conjunction with a lower n_{up} or vice versa (e.g., C-2 and C-3 in Fig. 3.6a), m is reduced compared to the worst case scenario. In those cases, we are less confident that the lines are actually wrong as such patterns occur occasionally even if the line takes the correct branch. For example, a C-2-like pattern can be caused by blunders in the DEM, while a C-3-like pattern can occur along the centerlines of larger glaciers. By using Equation 3.7 we allocate fewer iterations to these possibly correct cases than to cases where we are more certain that they are actually wrong (C-1).

Tests indicate that many wrong centerlines shift to the correct branch within less than five iterations. Thus, we limit the maximum number of iterations m_{max} to five, no matter the magnitude of n_{up} and Δz_{up} . Not obtaining a better solution after five iterations may indicate wrong divides (i.e., glaciers are not split correctly, and the centerline has to flow over a divide) or problems with the DEM (i.e., blunders within a large area that can not be bypassed). A narrow branch located next to a very wide branch may also prevent a correct solution within five iterations. However, even if the algorithm found the correct branch after more than five iterations, the resulting line likely had an implausible shape due to the high b value (Fig. 3.4d).

Fig. 3.6b shows a typical example of the progression of Δz_{up} during the optimization procedure, in case there is a better branch option: Δz_{up} remains high during the first three iterations because the centerline keeps taking the wrong branch. In iteration four, the centerline shifts to the correct branch and Δz_{up} decreases significantly. This drop in Δz_{up} is typically associated with a drop in n_{up} (not shown in Fig. 3.6b), which results in a lower m according to Fig. 3.6a. In most cases, the number of accomplished iterations is higher than the new m , and therefore, the optimization terminates as soon as the centerline shifts to the correct branch.

To obtain Δz_{up} and n_{up} , we sample the DEM only along the uppermost 25% of the centerlines' length. Centerlines most often take the wrong route (i.e., flow upslope) in this uppermost glacier section, where the different glacier branches tend to be interconnected. The same is very unlikely in the lowermost glacier part, as there is typically only one branch left. Even if more than one branch is left, these branches are generally separated by nunataks that can not be crossed by centerlines. Moreover, upslope flow in the uppermost glacier part is clearer evidence of a wrong route than upslope flow in lower parts, where the surface may be more irregular, for example, due to varying debris coverage. Including lower glacier parts could lead to large Δz_{up} and n_{up} values although the centerline takes the correct route.

Following the optimization, the best solution is selected from the calculated centerlines. We choose the solution that has the smallest n_{up} . If two or more solutions have the same n_{up} , we order them according to Δz_{up} and choose the one with the smallest Δz_{up} . If this does not lead to a unique solution either, we take the one solution with the lowest iteration number. Selection of the best solutions yields the final set of glacier centerlines.

Fig. 3.7a (corresponding to Fig. 3.4a) shows the preliminary set of centerlines as derived for Gilkey Glacier, while Fig. 3.7b shows the optimized set of glacier centerlines. The three red circles indicate implausible centerlines with significant upslope flow that are successfully adapted during the optimization step. The orange circle shows an implausible centerline that is not improved because there is no upslope flow in this case (the optimization does not respond because Δz_{up} and n_{up} are zero). In Fig. 3.7b, the blue bold numbers indicate which iterative solution is chosen as the best solution. In 55 cases, this is the initial solution '0' or solution '1'; in 22 cases, higher order solutions are picked.

The derived centerlines reach all the way from the glacier heads to the glacier termini. If two or more branches converge, lines start to overlap. As the optimization step can

result in different b values for each individual centerline, the derived centerlines do not necessarily overlap perfectly. The green circle in Fig. 3.7b shows an example of imperfect overlap in case of Gilkey Glacier.

3.5.3 Step 3 – Derivation of branches and branch order

The ultimate goal of this step is to remove the overlapping sections of the centerlines and to arrive at individual branches that are classified according to a geometric order. We keep the longest centerline that reaches from the head to the terminus. The remaining centerlines are trimmed so that they reach from their head to the next larger branch. If a trimmed centerline falls below a length threshold, it is deleted.

3.5.3.1 Branches

We consider the longest centerline as the main branch, following previous studies (Bahr and Peckham, 1996; Paul et al., 2009). This main branch is exported into a separate file. Then, from the initial file, we remove the main branch including line segments within a distance k (m) of the main branch (Fig. 3.7c). We apply this minimum distance k because different b values, employed during the optimization step, can yield centerlines that do not overlap perfectly. Centerlines may run in parallel in the same branch before they converge, or they may diverge again, after having converged higher on the glacier. k , defined according to Equation 3.8, allows for eliminating such cases of imperfect overlap.

$$k = \begin{cases} w_1 \cdot S + w_2 & : k \leq k_{\max} \\ k_{\max} & : k > k_{\max} \end{cases} \quad (3.8)$$

The constants w_1 , w_2 and k_{\max} are given in Table 3.1. Larger glaciers tend to have wider branches and parallel running centerlines in the same branch may be farther apart. To account for this, we increase k as a function of S . k is not the actual branch width, but rather a minimum distance that is required to eliminate cases of imperfect overlap.

The application of k may yield lines that are split into multiple parts (one segment from the head to the first conversion point, the second segment from the first to the second conversion point, etc.). As the segment from the first conversion point to the terminus is already covered by the main branch, we keep only the one segment in contact with the glacier head and remove all the other segments.

The step above is applied iteratively to the longest centerline of the updated initial file until the number of remaining centerlines reaches either zero or their length falls below a certain length. As a length threshold, we reapply r defined in Equation 3.1. In cases where r would remove all centerlines (which may occur for small glaciers), Equation 3.1 is not applied. Instead, r adopts the length of the longest centerline.

Merging of the identified individual branches yields the final set of branches. In case of Gilkey Glacier, 53 branches are obtained; 24 out of 77 lines are omitted because their length is below r . In Fig. 3.7c, the heads of omitted branches are marked in orange. The green circle in Fig. 3.7c shows an area of initially imperfect overlap after employment of step 3.

3.5.3.2 Branch order

The above step yields a set of branches for every glacier and also establishes a branch order using the branch length as a criterion: while the longest branch is the main branch (highest-order), the shortest branch is the lowest-order branch. Next, we evaluate the number of side branches that contribute to each individual branch. In this case, the branch order increases with the number of contributing branches. This results in main branches that have the highest numbers allocated. The numbers decrease as the branches fork into smaller branches. '1' stands for the lowest-order branch, meaning that there are no other branches flowing into this corresponding branch. The applied branch order is derived from the stream order proposed in Shreve (1966) and gives some first-order information about the branch topology of the glacier.

The implementation consists of a proximity analysis that is iteratively applied to each individual branch. We start by allocating an order of one (lowest-order) to every branch. Next, we iterate through the branches in the order of increasing length and flag the branches that are within a distance of k (Equation 3.8) from the one branch selected at that iteration step (the reference branch). The proximity analysis is applied only within the glacierized terrain, that is, a branch separated by nunataks is not flagged unless k is exceeded at a point without nunatak between branch and reference branch. By summing the individual orders of the flagged branches, we arrive at the true order of the selected reference branch. This true order is updated instantaneously because its updated value is required for the next iterations.

Fig. 3.7d shows the result for Gilkey Glacier. The '53' of the main branch indicates that 53 first-order branches converge to make up the main branch.

3.5.4 Quality analysis and manual adjustments

The quality analysis consists of a visual check, conducted throughout the domain by evaluating the derived centerlines in conjunction with contours (50 m contour spacing), shaded relief DEMs, and satellite imagery (mostly Landsat). A 25 km × 25 km grid, covering the entire study area, is used for guidance and keeping track of checked regions. We assess whether heads and termini are located correctly. For the termini, this means approximately at the center of the tongue; for the heads, at the beginning of a branch. The actual centerlines should flow roughly orthogonal to contour lines and parallel to visible moraines.

Glacier termini are moved to the center of the tongues, and glacier heads are added, deleted or moved as needed. To determine the number of moved termini, we compare the coordinates of the initial, automatically derived termini to the coordinates of the checked termini and sum the number of cases with changed coordinates. A similar analysis allows us to distinguish and quantify the two categories 'added' and 'deleted' heads.

Instead of editing the actual centerlines manually, we establish a new set of lines that we call 'breaklines'. The idea is to treat these breaklines like nunataks upon rerunning of step 2 of our workflow. This implies that centerlines may not cross breaklines; moreover, breaklines change the derived penalty raster. Such an approach allows for efficient correction of wrong centerlines. For example, it is useful to adapt a centerline that did not shift into the correct branch despite the optimization procedure. A simple breakline that blocks access to the wrong branch is sufficient to reroute the wrong centerline, which is much faster than manually editing the actual centerline. In the context of the quality analysis, counting the number of set breaklines allows for quantifying wrong centerlines.

To obtain the final set of centerlines, steps 2 and 3 of the workflow are repeated using the adapted heads, termini and breaklines as input, without changing any of the remaining input data or parameters. To allow breaklines as an additional input, an adapted version of the code of step 2 is run.

3.5.5 Comparison to alternative methods

To identify differences between alternative methods, it would be ideal to compare the actual centerline shapes. However, quantitatively assessing shape agreement is challenging, especially for a large number of glaciers. Here, we use the length as a proxy for agreement and carry out two comparisons. First, we compare the glacier lengths derived from

a hydrological approach to the lengths derived from our longest centerlines. To obtain the hydrological lengths, we run the tool 'Flow Length' from the ESRI ArcGIS® software package, which is similar to the tool applied by Schiefer et al. (2008). While this tool yields a length parameter for every glacier, it does not output an actual line that can be checked visually.

In the second comparison, we evaluate agreement between our longest centerlines and our centerlines between highest and lowest glacier elevations. This comparison yields apparent length differences that would occur by applying an approach that considers only the highest glacier elevations as heads (e.g., following Le Bris and Paul, 2013), rather than an algorithm that considers multiple heads. Unlike in the first experiment, we do not compare two approaches that are fundamentally different, but rather the same approach with one different assumption regarding glacier heads. Thus, we expect better agreement in the second experiment.

3.6 Results

For the 21,720 glaciers with an area $> 0.1 \text{ km}^2$, we obtain 41,860 centerlines, of which 8480 have a non-zero optimized iterative solution. The centerlines range in length between 0.1 and 195.7 km; the summed length is 87,460 km. Mean glacier length of our sample, as derived from the respective longest centerlines, is 2.0 km. 4350 glaciers have more than one branch and the corresponding branch orders reach up to 340.

Fig. 3.8 shows the centerlines derived for the Stikine Icefield area, located in the Coast Mountains of southeast Alaska / northwest Canada. The glacier geometries range from large outlet glaciers to medium-sized valley and small cirque glaciers.

Table 3.2 gives an overview of the manual changes conducted during the quality analysis. 19,060 of the 21,720 glaciers (87.8%) require no manual intervention at all. 2660 glaciers (12.2%) need any kind of manual intervention within the three-step procedure. Most cases of manual intervention are required to adapt the automatically derived glacier heads (1850 deleted, 1070 added) and termini (770 moved), indicating that steps 1 or 3 do not yield the expected outcome in these instances. 580 breaklines are used to adjust the course of the actual centerlines, indicating that in these cases, step 2 does not yield the intended result.

3.7 Discussion

3.7.1 Algorithm

Despite its empirical nature, our approach yields plausible results for a wide range of glacier sizes and shapes, provided both good quality DEMs and glacier outlines are available. However, the algorithm has limitations, as shown by the quality analysis. The main challenge is to automatically derive glacier heads and termini, due to the large natural variability inherent in the glacier sample with respect to size, shape and hypsometry. The actual derivation of the centerlines is less error-prone.

3.7.1.1 Termini

We use the lowest glacier points to automatically identify glacier termini, which can lead to problems described in Le Bris and Paul (2013). Especially if glacier tongues reach low-slope terrain, which is typical for expanded-foot and piedmont glaciers, the lowest glacier cell may not be located in the center of the glacier tongue, but rather along the side of the glacier. This ‘pulls’ the line away from the glacier center and leads to centerlines that are not realistic. Although this inconsistency only affects the immediate tongue area, it may interfere with certain applications and thus requires a manual shift of the terminus. In our study area, shifting of misplaced termini accounts for a considerable number of cases requiring manual input (Table 3.2). Currently, we do not have a reliable automatic approach to detect and adapt such misclassified termini.

In many glacierized areas, there are glaciers that drain into multiple tongues. Our algorithm identifies the lowest point as the only terminus and therefore does not account for multiple termini. To address this problem, we have to manually split these glaciers into separate catchments (i.e., one catchment per tongue), followed by treating the catchments like separate glaciers. In Alaska and northwest Canada, only a handful of glaciers drain into multiple tongues, therefore, the amount of manual intervention remains relatively small.

3.7.1.2 Heads

By definition, our algorithm obtains exactly one point per local elevation maximum. The corresponding centerline covers one branch, other branches that may originate from the same area remain without centerlines. This is illustrated in Fig. 3.7b, where not all branches

have a centerline allocated. Because our algorithm does not necessarily yield centerlines for each individual glacier branch, additional heads may have to be set manually, often combined with breaklines (required to prevent centerlines from clustered heads taking the same branch). In our test area, this constraint is responsible for most cases in the category ‘added heads’ (Table 3.2). Glaciers that fork from one into multiple branches, such as glaciers on volcanoes, are most susceptible to the problem.

We further prescribe that centerlines must run from their head to the terminus. While this is appropriate for many glacier geometries, it may not be the case for hanging or apron glaciers. For example, the minimum point of a small, wide apron glacier may be on one side, while a local maximum may be on the other side of the glacier. This results in a centerline that runs almost parallel to the contours, yielding a maximum length that is too long. In such cases, manual intervention is required to remove implausible head-terminus constellations. In our test area, this problem is responsible for the bulk of corrections with regard to deleted heads (Table 3.2). A simple, yet promising approach is the filtering of the derived centerlines using slope (or alternatively, a ratio between Δz_{up} and the corresponding Δz_{down} measured along the centerlines). Implausible centerlines tend to have very low slope and could thus be removed in an automated manner, thereby reducing the error numbers in Table 3.2. However, more work is required to test the feasibility of this filtering approach. Alternatively, by applying a higher minimum glacier area threshold (e.g., 1 km² instead of 0.1 km²), the amount of manual corrections could be reduced, as the challenging glacier geometries tend to have small areas.

3.7.1.3 Cost grid – least cost route approach

Our algorithm generally yields plausible centerlines if we derive the routes from cost grids established with a and b values of 4.25 and 3.5, respectively (Equation 3.2). The Euclidean distance term controls this initial cost grid, reflecting our assumption that the main flow occurs in the glacier center. If this assumption does not hold, the quality of the resulting centerlines may decline, although we consider elevation in Equation 3.2 and also conduct an optimization step. Lower quality centerlines are found, for example, on glaciers that drain very wide, asymmetric basins. In contrast, our quality analysis indicates that the approach works particularly well for valley glaciers. Alaska and northwest Canada comprise many outlet and valley glaciers, which is an important reason for the relatively high success rate in this area (Table 3.2).

The existence of nunataks tends to improve the derived centerlines. Due to the high penalty values close to the nunataks, centerlines are forced to flow around nunataks, which is typically consistent with their expected course, though this is not the case for glaciers with seracs that may discharge over nunataks. In our test area, nunataks are abundant, which simplifies the application of the cost grid – least cost route approach.

Equation 3.2 is only one way to obtain a functioning cost grid. Other, possibly shorter equations may yield similar results. For example, it would be possible to use the same values for f_1 and f_2 upon recalibrating a and b , thus reducing the number of variables by one. Instead of exponentials, one could also attempt to obtain a cost grid using logarithms.

3.7.1.4 Optimization

The optimization is a crucial element of the cost grid – least cost route approach and works robustly in general. We identify three cases where the optimization either fails or does not respond at all. First, no optimization occurs if the line continuously flows downslope, despite taking the wrong route (m in Equation 3.7 is zero in these cases). Second, the algorithm does not optimize if the upslope flow occurs below the upper 25% of the centerline’s length (Δz_{up} and n_{up} are only determined within the first 25%). An m that is not high enough (despite detected upslope flow) is a potential third cause for failure of the optimization. It is difficult to attribute wrong branches to individual cases; however, we hypothesize that the first case causes the largest number of errors.

The presented optimization is the result of experimenting with different optimization approaches and break criteria. Intuitive break criteria such as ‘optimize until Δz_{up} and n_{up} equals zero’ or ‘optimize until improvement of Δz_{up} and n_{up} equals zero’ do not work reliably due to the large variability inherent in the glacier sample. For example, a solution may decline temporarily (resulting in higher Δz_{up} or n_{up}) before it improves again to finally yield the best solution. Iteratively calculating all the solutions according to Equation 3.7 and then choosing the best solution out of this set of centerlines generally is most successful.

3.7.1.5 Branches and geometry order

The proposed approach to derive branches from centerlines works satisfactorily in most cases; however, we rely on various simplifications. For example, Equation 3.8 defines a

constant k for each glacier, which is then used to split the centerlines into branches. Ideally, k would correspond to the actual local branch width and thus evolve along each individual branch. While such a procedure is easily implementable for simple glacier geometries, it is very difficult in areas with many interconnected branches, and thus not implemented here. Assuming a constant k is most problematic for large glaciers, where the branch widths can vary from less than one to several tens of kilometers. In conjunction with the constant minimum length threshold r (Equation 3.1), the constant k may lead to branches that are omitted although they should not be, and vice versa. For large glaciers, such errors can be an important contributor to the categories ‘added’ and ‘deleted’ heads (Table 3.2).

3.7.2 Influence of DEM and outline quality

Our results depend on the quality of DEM and glacier outlines. While systematic elevation biases (e.g., like those found in the SRTM DEM) have little to no effect, blunders such as bumps (e.g., found in the ASTER GDEM2, due to a lack of contrast in the corresponding optical imagery) are more severe. They lead to elevation maxima that are not real, which interferes with our search for actual glacier heads. Blunders also affect the course of the centerlines. Artificial bumps lead to upslope flow and the subsequent optimization picks centerlines that flow around these bumps. These solutions are better according to the optimization criteria Δz_{up} and n_{up} , but in reality may be worse than the initial solutions. In areas where we rely on DEMs with blunders, the DEM quality is responsible for most manual corrections in any error categories.

If the glacier is part of a larger glacier complex, correct ice divides along the actual drainage divides as retrieved from the DEM are crucial. In case of erroneous divides, centerlines flow over the divide, which may prompt an optimization although the only solution is to adapt the divides. Likewise, it is important to identify correctly location and shape of nunataks. In case of omitted nunataks, the centerlines may cross the nunataks, which is not intended. Identifying nunataks where there are none (e.g., on a central moraine) leads to centerlines flowing around these apparent nunataks, yielding an implausible curvy shape.

3.7.3 Quality assessment

For the quality assessment, we use shaded relief DEMs, contour lines, and satellite imagery. As moraines and contour lines are only a proxy for ice flow direction, it would be ideal to consult actual velocity field data to validate the centerlines. However, at the time of the quality analysis, such flow fields were not available on a larger scale. Recently presented data (Burgess et al., 2013) may be used for future studies.

Visual assessments involve some degree of subjectivity, which we attempt to minimize by checking the results multiple times. Comparison to centerlines exclusively derived by hand could extend the current quality assessment. However, to be meaningful, such tests should comprise multiple glaciers from each glacier type, manually processed by different technicians. This is very time-consuming and thus beyond the scope of this study.

3.7.4 Comparison to alternative methods

To quantify method-related differences, we compare the glacier lengths derived from alternative algorithms. A meaningful analysis is supported by the large number of length observations available. Calculating the ratios of the lengths obtained from different methods allows a better comparison of the results from individual glaciers. The histogram in Fig. 3.9a illustrates the length differences arising from the concurrent application of our cost grid – least cost route and a hydrological approach. The distribution of the obtained ratios is shown in the histogram in Fig. 3.9a. While the mean and median are very close to unity ($\bar{R} = 0.99$, $R_{50} = 1.02$), the distribution is left-skewed with a maximum between 1.05 and 1.15 and considerable spread. Only ~50% of the 21,720 glaciers have lengths that are within 10% of each other. Assuming that the centerlines from our cost grid – least cost route approach are the ‘correct’ reference, the distribution peak between 1.05 and 1.15 confirms the finding of Schiefer et al. (2008) that hydrological approaches tend to overestimate glacier length due to the deflection of the hydrological ‘flowline’ to the glacier edge in convex areas. However, in almost 50% of the cases, the lengths from the hydrological approach are shorter than the lengths from the cost grid – least cost route approach. The pattern is found throughout all size classes and can occur if the hydrological flowline not only gets deflected in areas with convex glacier geometry, but actually leaves the glacier before reaching the lowest glacier elevation. In these cases, the hydrological approach may underestimate glacier length. In the cost grid – least cost route approach, every centerline

is forced to reach the lowest glacier elevation, an assumption that may not always hold, which then leads to an overestimation of the length by our approach. Combined, the two tendencies for under- and overestimation may explain the considerable fraction of ratios between 0.7 and 0.9.

The histogram in Fig. 3.9b shows how different the lengths would be if centerlines were computed between the lowest and highest glacier elevations only (e.g., Le Bris and Paul, 2013), instead of considering multiple branches per glacier. For this comparison, we extract only the 4350 glaciers that have two or more centerlines, as the two lengths must be identical in case of the remaining 17,370 glaciers. Excluding the glaciers with one centerline tends to exclude the smallest glaciers, thus, nearly all glaciers $< 0.5 \text{ km}^2$ are omitted. More than 70% of the glaciers have a high ratio between 0.95 and unity, meaning that the centerline originating from the highest glacier elevation has a length that is within 5% of the longest centerline's length. For most glaciers, the longest centerline is actually identical to the line between the lowest and the highest glacier elevation, which is explained by a strong correlation of elevation range and length. Nevertheless, considerable outliers may occur in individual cases, especially for large glaciers that have many branches.

3.8 Conclusions

We have developed a three-step algorithm to calculate glacier centerlines in an automated fashion, requiring glacier outlines and a DEM as input. In the first step, the algorithm identifies glacier termini and heads by searching for minima and local elevation maxima along the glacier outlines. The second step comprises a cost grid – least cost route implementation, which forces the centerlines towards both the central portion and lowest elevations of the glacier. The second step also implements an optimization routine, which obtains the most plausible centerlines by slightly varying the cost grid. In the third step, the algorithm divides the centerlines into individual branches, which are then classified according to branch order (Shreve, 1966).

We have developed and applied our centerline algorithm on a glacier inventory for Alaska and northwest Canada (Arendt et al., 2013). The algorithm is applied to 21,720 glaciers with a minimum area of 0.1 km^2 , yielding 41,860 individual branches ranging in length between 0.1 and 195.7 km. The mean length of the glacier sample is 2.0 km. Our quality analysis shows that the majority (87.8%) of the glaciers required no manual corrections. The most common errors occurred due to misidentification of either glacier heads

or termini (5.5% and 3.5% of errors, respectively). Once heads and termini are correctly identified, the algorithm determines centerlines for nearly all (98.6%) cases. The quality analysis further indicates that the algorithm works best for valley glaciers, while apron glaciers tend to be most challenging. Improvements of the algorithm, such as detection of implausible centerlines by using a slope threshold, may reduce the amount of manual intervention in the future.

For our sample of 21,720 glaciers, we compare the lengths derived from a hydrological approach (e.g., Schiefer et al., 2008) to the lengths derived from our longest centerlines. We find considerable variation: although the average ratio of the two lengths is close to unity, only ~50% of the glaciers have the two lengths within 10% of each other. This suggests that the choice of the applied method may significantly influence the derived glacier lengths. Comparing the lengths from the centerline between highest and lowest glacier elevations to the lengths from the longest centerlines shows that they agree well: >70% of the glaciers with two or more branches have the two lengths within 5% of each other. Agreement is best for small glaciers with few branches. Our results suggest that the centerline between the highest and the lowest glacier point is generally valid to describe the glacier length although considerable outliers may occur in individual cases.

The derived results do not provide a unique, 'true' solution. The results may vary with the parameters chosen in the applied equations; moreover, technician interpretation adds subjectivity within the quality analysis. Nevertheless, the proposed approach contributes towards a standardized derivation of centerlines. The final product may be used, for example, to calculate the glacier length using both suggested methods (Paul et al., 2009) or to conduct topological analyses (Bahr and Peckham, 1996). It may also be used for area-length scaling applications (Schiefer et al., 2008) or as input for flowline modeling (Sugiyama et al., 2007). As soon as good quality DEMs and glacier outlines are globally available, the scope of the presented project may be expanded from a regional to a global scale.

3.9 Acknowledgements

The work was supported by grants from NSF (#EAR 0943742) and NASA (#NNX11AF41G, #NNX11AO23G).

Table 3.1. Used parameter values and units

Symbol	Value	Unit	Equation
q_1	2×10^{-6}	m^{-1}	3.1
q_2	500	m	3.1
r_{\max}	1000	m	3.1
f_1	1000	-	3.2
f_2	3000	-	3.2
a	3.5	-	3.2
b	4.25*	-	3.2
Δb	0.1	-	optimization
u_1	2×10^{-6}	m^{-1}	3.4
u_2	200	m	3.4
l_{\max}	400	m	3.4
j_1	0.1	m^{-j_2}	3.7
j_2	0.7	-	3.7
m_{\max}	5	-	3.7
w_1	1×10^{-6}	m^{-1}	3.8
w_2	150	m	3.8
k_{\max}	650	m	3.8

* initial value, subject to optimization

Table 3.2. Manual changes attributed to individual error categories. Percentages are relative to the total of each category (e.g., deleted heads vs. total heads)

Category	Number	%
Total termini	21,720	
Moved termini	770	3.5
Total heads	53,210	
Deleted heads	1850	3.5
Added heads	1070	2.0
Total centerlines	41,860	
Breaklines	580	1.4
Total glaciers	21,720	
Glaciers with changes	2660	12.2

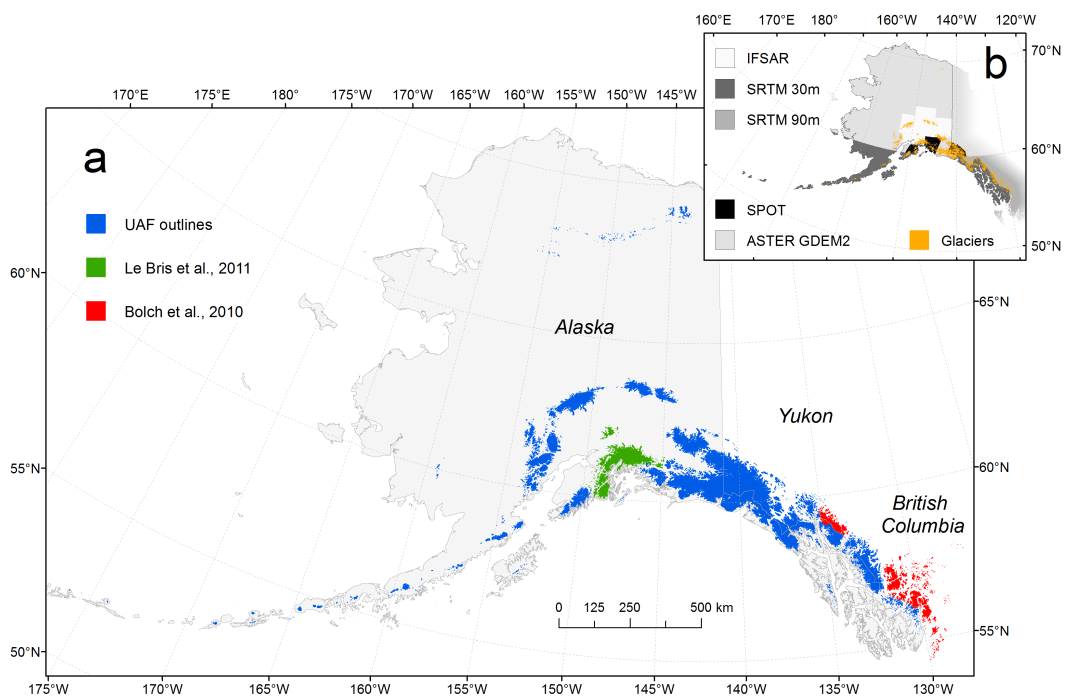


Figure 3.1. The study area comprising glaciers of Alaska and adjacent Canada. a) The three main outline sources marked in colors. b) The DEM products used within the study.

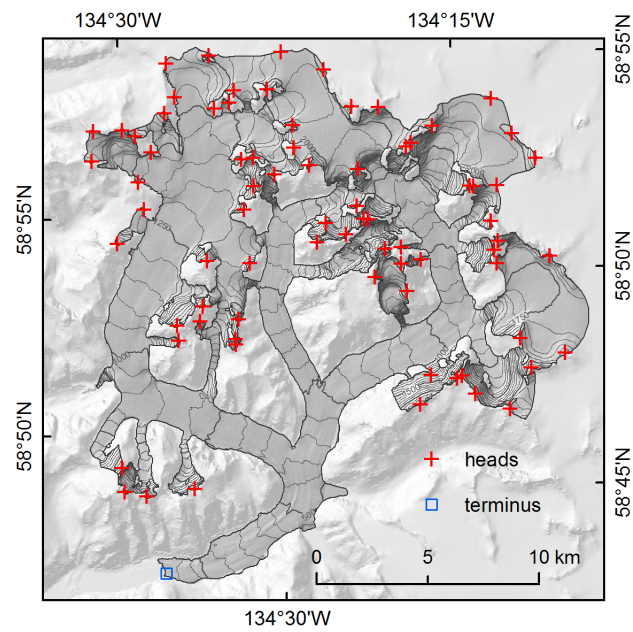


Figure 3.2. Automatically derived glacier heads (red crosses) and terminus (blue square) on Gilkey Glacier, Juneau Icefield, southeast Alaska. The 50 m contours and the shaded relief background are derived from the SRTM DEM.

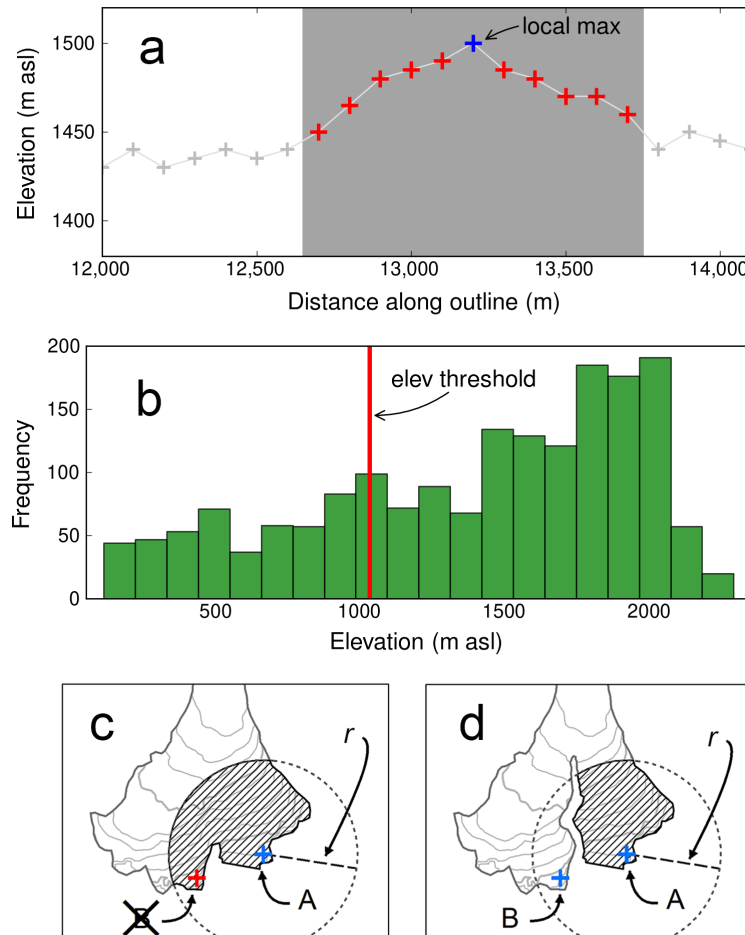


Figure 3.3. Three-step procedure to identify the heads of major glacier branches. a) Identification of local maxima along the glacier outline by comparing each point to its five neighbors in each direction. b) Histogram of the elevation distribution of all sampled points along the glacier outline. Only points above the elevation threshold are retained. c, d) Glacier area covered by circle with radius r around identified head A; heads A and B are separated by less than r . In case c), head B (with lower elevation than head A) is eliminated. In case d), both heads are retained because the nunatak completely separates the two heads (i.e., splits the circle into two disconnected parts).

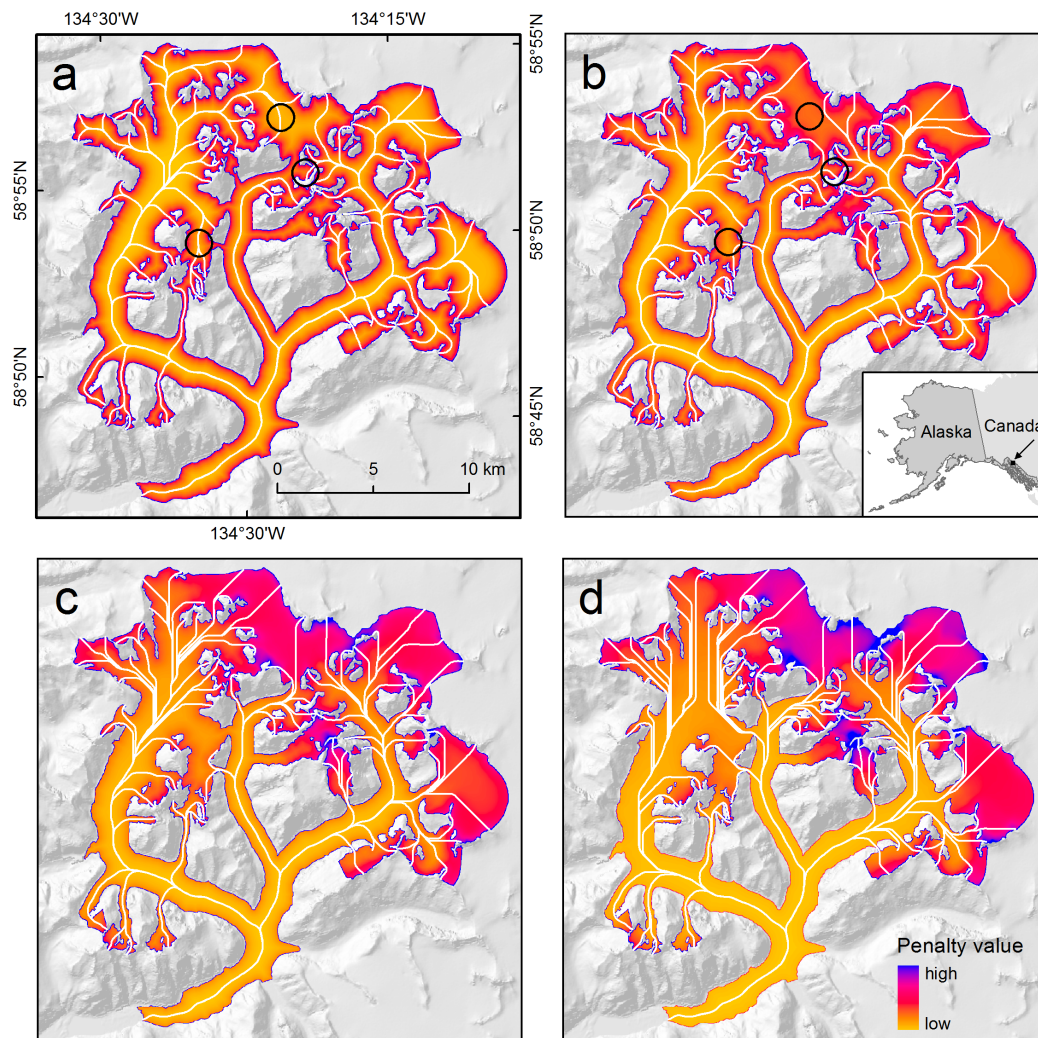


Figure 3.4. Selected penalty grids of Gilkey Glacier and corresponding centerlines, using a constant a value of 4.25, but varying b . a) Initial cost grid with $b = 3.5$. The penalty values strongly decrease towards the center of the branches. There is a subsidiary decline from higher to lower elevations. The black circles indicate centerlines that take implausible routes with significant upslope flow. b) The penalty grid after two iterations with $b = 3.7$. The initially wrong centerlines now take the correct routes, however, other centerlines have partially deviated from their expected courses. c) Four iterations, $b = 3.9$. d) Six iterations, $b = 4.1$ (not allowed during the optimization). Many centerlines are cutting corners, especially in higher glacier reaches.

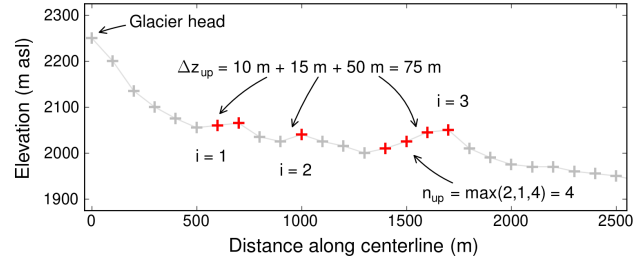


Figure 3.5. Elevation profile along a glacier centerline illustrating the definition of Δz_{up} and n_{up} for $I = 3$ sections.

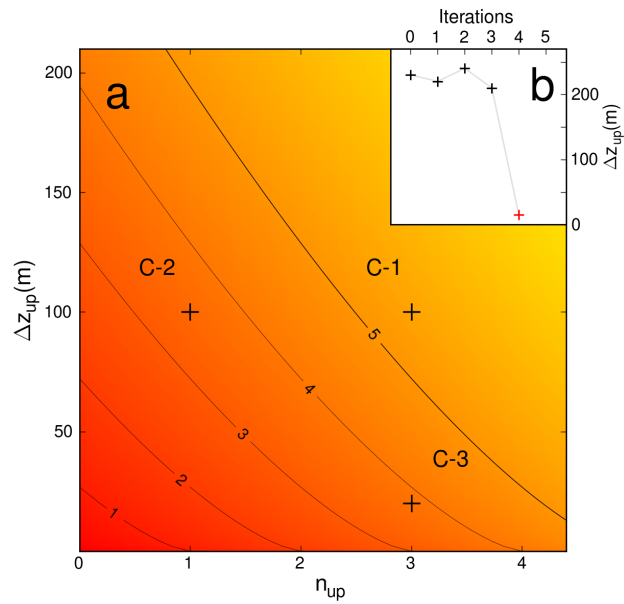


Figure 3.6. Illustration of the applied iteration threshold. a) The maximum number of iterations, m (colored surface and contours), as a function of the number of samples with continuous elevation increase, n_{up} , and the total elevation increase, Δz_{up} . b) Typical progression of Δz_{up} during the optimization procedure, in a case where there is a better branch option.

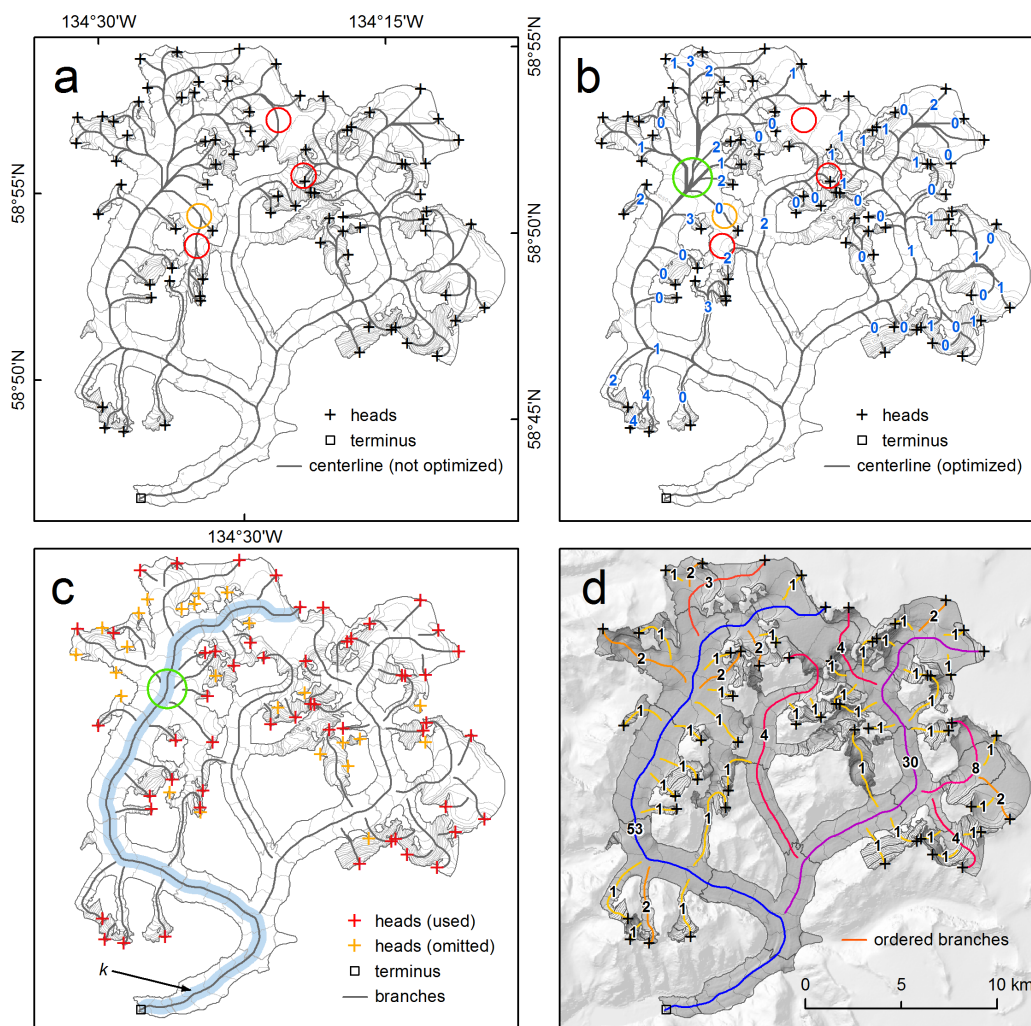


Figure 3.7. The main processing steps illustrated using the example of Gilkey Glacier, Juneau Icefield. a) The grey lines show the centerlines derived without the optimization step, using $a = 3.5$ and $b = 4.25$ (Equation 3.2). Red and orange circles mark implausible centerlines. b) Centerlines after the optimization step. The lines indicated by red circles are improved, while the line indicated by the orange circle remains unchanged. Blue bold numbers show the final iterative solutions for selected centerlines (e.g., '3' means solution of iteration three). The green circle marks an area of imperfect overlap after optimization of the centerlines, which is due to the different applied b values. c) Branches after splitting the centerlines. The width of the blue area illustrates k (Equation 3.8). Overlapping parts (green circle) are eliminated and short segments (belonging to the orange heads) are omitted. d) Branches after allocation of geometric order. The order number indicates the number of first-order branches flowing into the corresponding branch.

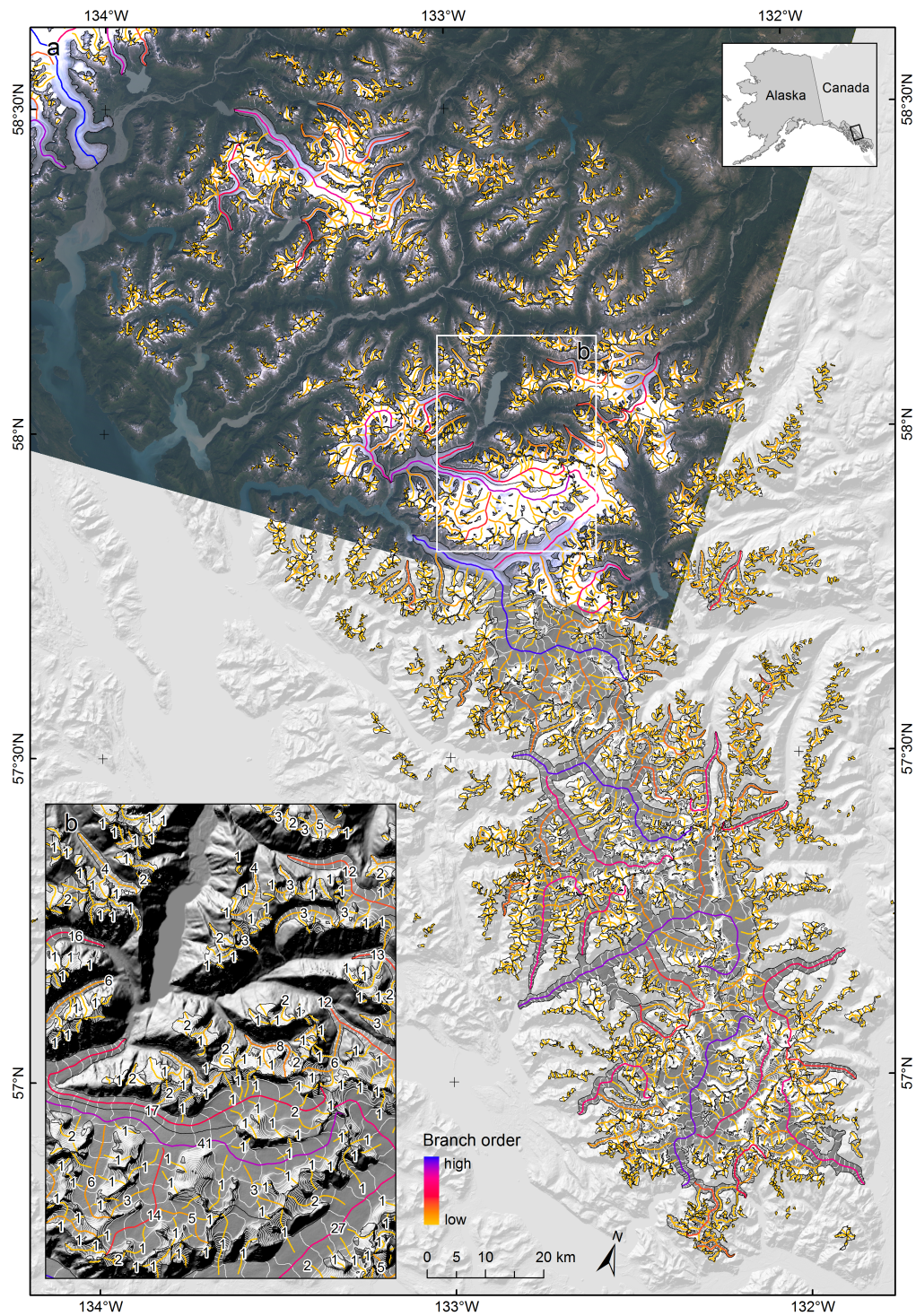


Figure 3.8. Derived centerlines for glaciers in the Stikine Icefield area. Line colors indicate branch order. The shaded relief background is computed from the SRTM DEM. 50 m contours are shown as white lines. Map a) includes a Landsat 5 Thematic Mapper true color composite from 2005/08/11 as reference (scene LT50570192005223PAC01). Inset b) shows a subarea with labels quantifying the branch order.

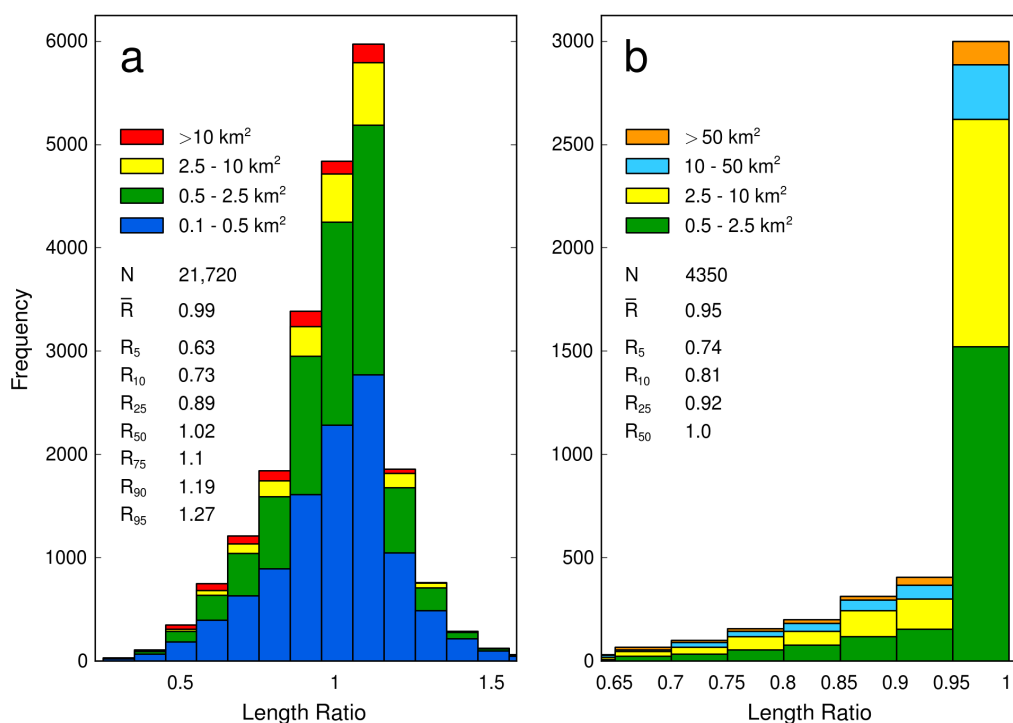


Figure 3.9. Histograms illustrating the length ratio distributions of differently derived glacier lengths. Colors distinguish size categories, N indicates the total number of observations. Mean (\bar{R}) and selected quantiles (R) are calculated for the complete distributions. Panel a) shows the ratio of length derived from a hydrological approach to the length derived from our longest centerline. Bar width is 0.1. Panel b) shows the ratio of length derived from the centerline between the highest and the lowest glacier elevation to the length derived from our longest centerline. Only glaciers with more than one centerline are considered. Bar width is 0.05.

References

- Arendt, A., A., T. Bolch, J. G. Cogley, A. Gardner, J. O. Hagen, R. Hock, G. Kaser, W. T. Pfeffer, G. Moholdt, F. Paul, et al. (2013). Randolph glacier inventory [v3. 0]: A dataset of global glacier outlines. *Global Land Ice Measurements from Space, Boulder, Colorado, USA. Digital Media*.
- Bahr, D. B. and S. D. Peckham (1996). Observations and analysis of self-similar branching topology in glacier networks. *Journal of Geophysical Research* 101(B11), 25511–25521.
- Bolch, T., B. Menounos, and R. Wheate (2010). Landsat-based inventory of glaciers in western Canada, 1985-2005. *Remote Sensing of Environment* 114(1), 127–137.
- Burgess, E. W., R. R. Forster, and C. F. Larsen (2013). Flow velocities of Alaskan glaciers. *Nature Communications* 4:2146.
- Farinotti, D., M. Huss, A. Bauder, M. Funk, and M. Truffer (2009). A method to estimate the ice volume and ice-thickness distribution of alpine glaciers. *Journal of Glaciology* 55(191), 422–430.
- Farr, T. G., P. A. Rosen, E. Caro, R. Crippen, R. Duren, S. Hensley, M. Kobrick, M. Paller, E. Rodriguez, L. Roth, D. Seal, S. Shaffer, J. Shimada, J. Umland, M. Werner, M. Oskin, D. Burbank, and D. Alsdorf (2007). The Shuttle Radar Topography Mission. *Reviews of Geophysics* 45(2), 1–33.
- Heid, T. and A. Kääb (2012). Repeat optical satellite images reveal widespread and long term decrease in land-terminating glacier speeds. *The Cryosphere* 6(2), 467–478.
- Korona, J., E. Berthier, M. Bernard, F. Rémy, and E. Thouvenot (2009). SPIRIT. SPOT 5 stereoscopic survey of Polar Ice: Reference Images and Topographies during the fourth International Polar Year (2007–2009). *ISPRS Journal of Photogrammetry and Remote Sensing* 64(2), 204–212.
- Le Bris, R. and F. Paul (2013). An automatic method to create flow lines for determination of glacier length: A pilot study with Alaskan glaciers. *Computers & Geosciences* 52, 234–245.
- Le Bris, R., F. Paul, H. Frey, and T. Bolch (2011). A new satellite-derived glacier inventory for Western Alaska. *Annals of Glaciology* 52(59), 135–143.

- Leclercq, P. W., P. Pitte, R. H. Giesen, M. H. Masiokas, and J. Oerlemans (2012). Modelling and climatic interpretation of the length fluctuations of Glaciar Frías (north Patagonian Andes, Argentina) 1639–2009 AD. *Climate of the Past* 8(5), 1385–1402.
- Li, H., F. Ng, Z. Li, D. Qin, and G. Cheng (2012). An extended “perfect-plasticity” method for estimating ice thickness along the flow line of mountain glaciers. *Journal of Geophysical Research* 117(F1), F01020.
- Linsbauer, A., F. Paul, and W. Haeberli (2012). Modeling glacier thickness distribution and bed topography over entire mountain ranges with glabtop: Application of a fast and robust approach. *Journal of Geophysical Research* 117(F3), F03007.
- McNabb, R., R. Hock, S. O’Neel, L. Rasmussen, Y. Ahn, M. Braun, H. Conway, S. Herreid, I. Joughin, W. Pfeffer, B. Smith, and M. Truffer (2012). Using surface velocities to calculate ice thickness and bed topography: a case study at Columbia Glacier, Alaska, USA. *Journal of Glaciology* 58(212), 1451–1464.
- Melkonian, A. K., M. J. Willis, M. E. Pritchard, A. Rivera, F. Bown, and S. A. Bernstein (2013). Satellite-derived volume loss rates and glacier speeds for the Cordillera Darwin Icefield, Chile. *The Cryosphere* 7(3), 823–839.
- Nuth, C., J. Kohler, M. König, A. von Deschwanden, J. O. Hagen, A. Käab, G. Moholdt, and R. Pettersson (2013). Decadal changes from a multi-temporal glacier inventory of svalbard. *The Cryosphere Discussions* 7(3), 2489–2532.
- Oerlemans, J. (1997a). A flowline model for Nigardsbreen, Norway: projection of future glacier length based on dynamic calibration with the historic record. *Annals of Glaciology* 24, 382–389.
- Oerlemans, J. (1997b). Climate Sensitivity of Franz Josef Glacier, New Zealand, as Revealed by Numerical Modeling. *Arctic and Alpine Research* 29(2), 233–239.
- Paul, F., R. G. Barry, J. G. Cogley, H. Frey, W. Haeberli, A. Ohmura, C. S. L. Ommanney, B. Raup, A. Rivera, and M. Zemp (2009). Recommendations for the compilation of glacier inventory data from digital sources. *Annals of Glaciology* 50(53), 119–126.
- Schiefer, E., B. Menounos, and R. Wheate (2008). An inventory and morphometric analysis of British Columbia glaciers, Canada. *Journal of Glaciology* 54(186), 551–560.

Shreve, R. L. (1966). Statistical Law of Stream Numbers. *The Journal of Geology* 74(1), 17–37.

Sugiyama, S., A. Bauder, C. Zahno, and M. Funk (2007). Evolution of Rhonegletscher, Switzerland, over the past 125 years and in the future: application of an improved flowline model. *Annals of Glaciology* 46, 268–274.

Tachikawa, T., M. Hato, M. Kaku, and A. Iwasaki (2011). Characteristics of aster gdem version 2. In *Geoscience and Remote Sensing Symposium (IGARSS), 2011 IEEE International*, pp. 3657–3660.

Chapter 4

General Conclusions

Sophisticated algorithms to split glacier complexes into single glaciers are a crucial link between the derivation of glacier complexes and the many applications that require individual glacier outlines as input. While there has been a wealth of research on the automation of glacier complex delineation, research with regard to the actual glacier separation has been rare. Our first algorithm contributes to the efforts to fill this gap. It allows us to separate glacier complexes into individual glaciers requiring two datasets as input that are available for most glacierized areas: a DEM and glacier complex outlines. The algorithm is based on hydrological modeling tools and identifies individual glaciers semi-automatically. Its application to Alaska ($>25,000 \text{ km}^2$ of ice, $\sim 98\%$ success rate) and southern Arctic Canada ($>40,000 \text{ km}^2$ of ice, $\sim 97\%$ success rate) indicates that the method is robust, requiring only a small number of manual corrections. The quality analysis further shows that the algorithm works best for valley glaciers, while ice caps are most challenging. Most misclassifications are due to sliver polygons, which not only occur due to failure of the algorithm, but also due to inaccuracies of the glacier complex outlines or DEMs.

Glacier centerlines are used for various glaciological applications, for example, calculating glacier lengths, conducting topological analyses, or flowline modeling. On a large scale, such applications have been hampered by the lack of available centerlines. Our second algorithm contributes to the solution of this problem. It applies a cost grid – least cost route approach that derives centerlines in an automated manner. This algorithm relies on glacier outlines (e.g., as derived from the first algorithm) and a DEM. In an initial step, termini and heads are derived for every glacier. Then, centerlines are derived by determining the least cost route on a previously determined cost grid. Finally, the resulting centerlines are split into branches, followed by the attribution of a branch order. The centerline algorithm is applied to 21,720 glaciers in Alaska, which corresponds to $86,400 \text{ km}^2$ of ice total, and accounts for more than 99% of the area of the Alaska glacier inventory. The algorithm performs well, yielding 41,860 individual branches. Most manual input is required to correct the automatically derived glacier heads ($\sim 5.5\%$) and termini ($\sim 3.5\%$), due to the large natural variability inherent in the glacier sample with respect to size, shape and hypsometry. The derivation of the centerlines is considerably less error-prone. Once erroneous heads and termini are corrected, only $\sim 1.4\%$ of the centerlines have to be edited. Our quality analysis indicates that the algorithm works best for valley glaciers, while apron glaciers

tend to be most challenging. A comparison with alternative approaches reveals that the derived lengths can vary significantly as a function of the algorithm used. The numbers obtained in the study predict the corresponding uncertainties for the first time.

Refinements of the presented algorithms, together with improved DEMs and outlines, are anticipated to further reduce the amount of manual intervention in the future. However, given the complicated nature of possible glacier geometries, it will remain challenging to develop fully automatic approaches that meet the same quality standards as approaches that allow some manual intervention. Nevertheless, as the required manual intervention is moderate, the scopes of the presented projects may be expanded from a regional to a global scale if more accurate DEMs and outlines become available globally. Ideally, this will contribute to the goal of having an accurate global glacier inventory that is evolving with the changing cryosphere. This, in turn, will improve our understanding of the cryosphere and its complex responses to global climate change.